

See discussions, stats, and author profiles for this publication at: <https://www.researchgate.net/publication/313034808>

# Direct and indirect climate change effects on carbon dioxide fluxes in a thawing boreal forest–wetland landscape

Article in *Global Change Biology* · January 2017

DOI: 10.1111/gcb.13638

CITATIONS

0

READS

387

6 authors, including:



**Manuel Helbig**

McGill University

20 PUBLICATIONS 75 CITATIONS

[SEE PROFILE](#)



**Laura Chasmer**

University of Lethbridge

99 PUBLICATIONS 1,696 CITATIONS

[SEE PROFILE](#)



**Ankur Desai**

University of Wisconsin–Madison

205 PUBLICATIONS 5,339 CITATIONS

[SEE PROFILE](#)



**Natascha Kljun**

Swansea University

100 PUBLICATIONS 3,082 CITATIONS

[SEE PROFILE](#)

Some of the authors of this publication are also working on these related projects:



Net radiative forcing of increasing methane emissions in a boreal forest-wetland landscape [View project](#)



Boreal Ecosystem Research and Monitoring Sites [View project](#)

MR. MANUEL HELBIG (Orcid ID : 0000-0003-1996-8639)

Received Date : 22-Oct-2016

Accepted Date : 26-Dec-2016

Article type : Primary Research Articles

**Direct and indirect climate change effects on carbon dioxide fluxes in a thawing boreal forest-wetland landscape**

**Manuel Helbig<sup>1\*</sup>, Laura E Chasmer<sup>2</sup>, Ankur R Desai<sup>3</sup>, Natascha Kljun<sup>4</sup>, William L Quinton<sup>5</sup>, Oliver Sonnentag<sup>1</sup>**

<sup>1</sup>*Université de Montréal  
Département de géographie & Centre d'études nordiques  
520 Chemin de la Côte Sainte-Catherine  
Montréal, QC H2V 2B8, Canada*

<sup>2</sup>*University of Lethbridge, Department of Geography, Lethbridge AB T1K 3M4, Canada*

<sup>3</sup>*University of Wisconsin-Madison, Department of Atmospheric and Oceanic Sciences, Madison, WI 53706, USA*

<sup>4</sup>*Swansea University, Department of Geography, Singleton Park, Swansea SA28PP, UK*

<sup>5</sup>*Wilfrid Laurier University, Cold Regions Research Centre, Waterloo ON N2L 3C5, Canada*

\*corresponding author:  
tel. 438-826-1985  
fax 514 343-8008  
email: manuel.helbig@umontreal.ca

**Keywords:** Climate change, Eddy covariance, Carbon dioxide, Boreal forest, Wetlands, Gross primary productivity, Ecosystem respiration, Permafrost

This article has been accepted for publication and undergone full peer review but has not been through the copyediting, typesetting, pagination and proofreading process, which may lead to differences between this version and the Version of Record. Please cite this article as doi:

10.1111/gcb.13638

This article is protected by copyright. All rights reserved.

Running head: *Climate impacts on NEE in boreal landscapes*

Submitted to: *Global Change Biology*  
*Primary Research Article*

## **Abstract**

In the sporadic permafrost zone of northwestern Canada, boreal forest carbon dioxide (CO<sub>2</sub>) fluxes will be altered directly by climate change through changing meteorological forcing and indirectly through changes in landscape functioning associated with thaw-induced collapse-scar bog (“wetland”) expansion. However, their combined effect on landscape-scale net ecosystem CO<sub>2</sub> exchange (NEE<sub>LAND</sub>), resulting from changing gross primary productivity (GPP) and ecosystem respiration (ER), remains unknown. Here, we quantify indirect land cover change impacts on NEE<sub>LAND</sub> and direct climate change impacts on modeled temperature- and light-limited NEE<sub>LAND</sub> of a boreal forest-wetland landscape. Using nested eddy covariance flux towers, we find both GPP and ER to be larger at the landscape- compared to the wetland-level. However, annual NEE<sub>LAND</sub> (-20 g C m<sup>-2</sup>) and wetland NEE (-24 g C m<sup>-2</sup>) were similar, suggesting negligible wetland expansion effects on NEE<sub>LAND</sub>. In contrast, we find non-negligible direct climate change impacts when modeling NEE<sub>LAND</sub> using projected air temperature and incoming shortwave radiation. At the end of the 21<sup>st</sup> century, modeled GPP mainly increases in spring and fall due to reduced temperature-limitation, but becomes more frequently light-limited in fall. In a warmer climate, ER increases year-round in the absence of moisture stress resulting in net CO<sub>2</sub> uptake increases in the shoulder seasons and decreases during the summer. Annually, landscape net CO<sub>2</sub> uptake is projected to decline by 25±14 g C m<sup>-2</sup> for a moderate and 103±38 g C m<sup>-2</sup> for a high warming scenario, potentially reversing recently observed positive net CO<sub>2</sub> uptake trends across the boreal biome. Thus, even without moisture stress, net CO<sub>2</sub> uptake of boreal forest-wetland landscapes may decline, and ultimately these landscapes may turn into net

CO<sub>2</sub> sources under continued anthropogenic CO<sub>2</sub> emissions. We conclude that NEE<sub>LAND</sub> changes are more likely to be driven by direct climate change rather than by indirect land cover change impacts.

## Introduction

The boreal biome, with its distinct land-atmosphere exchange of sensible heat, water vapor, methane, and carbon dioxide (CO<sub>2</sub>), plays an important role in the global and regional climate systems (Chapin *et al.*, 2000). For example, boreal forests represent an important carbon (C) sink of about 0.5 Pg C yr<sup>-1</sup> (Pan *et al.*, 2011), equivalent to 17±6 % of the global land CO<sub>2</sub> sink (Le Quéré *et al.*, 2015). Climate warming in the boreal biome of northwestern North America has caused widespread permafrost thaw at the southern permafrost limit inducing wetland expansion leading to replacement of boreal forests in lowland regions (e.g.; Helbig *et al.*, 2016a; Lara *et al.*, 2016; Chasmer & Hopkinson, in press). Previous studies have shown that land cover changes in these regions affect regional land-atmosphere interactions by favoring the partitioning of available energy to latent instead of sensible heat (Helbig *et al.*, 2016b) and by enhancing landscape methane emissions (Helbig *et al.*, in press). However, it remains uncertain how climate warming and resulting land cover changes influence net ecosystem CO<sub>2</sub> exchange (NEE), and its component fluxes gross primary productivity (GPP) and ecosystem respiration (ER) (Schuur *et al.*, 2015).

Along the southern limit of the North American permafrost zone, long-term net CO<sub>2</sub> uptake has resulted in large organic C stocks as peat (Robinson & Moore, 1999; Tarnocai *et al.*, 2009; Treat *et al.*, 2016). In these organic-rich boreal landscapes, thawing permafrost makes previously frozen organic C stocks available for decomposition and ER may be enhanced by

warming soils (Schuur *et al.*, 2009; O'Donnell *et al.*, 2012; Natali *et al.*, 2014; Treat *et al.*, 2014; Koven *et al.*, 2015). However, permafrost thaw in organic- and ice-rich landscapes often leads to surface subsidence and increased land surface wetness (e.g.; Osterkamp *et al.*, 2000; Baltzer *et al.*, 2014). Under saturated and anoxic conditions, associated with subsidence, organic matter decomposes more slowly, causing only an attenuated post-thaw increase in ER (Knoblauch *et al.*, 2013). At the same time, GPP might increase due to increased nutrient and soil moisture availability, and warmer soil and air temperatures (e.g.; Turetsky *et al.*, 2000; Camill *et al.*, 2001; Wickland *et al.*, 2006; Turetsky *et al.*, 2007; Keuper *et al.*, 2012; Finger *et al.*, 2016). The combination of changes in both GPP and ER in a warming climate will eventually determine if organic-rich boreal landscapes will continue to be long-term CO<sub>2</sub> sinks exerting a climate cooling effect (Frolking *et al.*, 2006). Since 1985, the land net CO<sub>2</sub> sink in the boreal biome (50° to 60° N, excluding Europe) increased by 8-11 Tg C yr<sup>-1</sup> (Welp *et al.*, 2016), but it remains unclear if this trend will continue in an increasingly warmer climate.

Recent warming trends in northwestern Canada, in the order of 0.25-0.50 °C per decade (DeBeer *et al.*, 2016), are likely to continue and potentially accelerate during the 21<sup>st</sup> century (Kirtman *et al.*, 2013). Direct climate change effects result from instantaneous ecosystem responses to these altered meteorological conditions. For example, boreal forest GPP is suppressed at air temperatures (T<sub>a</sub>, °C) below the freezing point and increases with both T<sub>a</sub>- and light-availability (Tanja *et al.*, 2003; Luyssaert *et al.*, 2007), while ER increases with T<sub>a</sub> and soil temperature (T<sub>s</sub>, °C) (Dunn *et al.*, 2007; Ueyama *et al.*, 2014). In addition to substantially warmer regional climates at high latitudes, future changes in cloud cover could alter incoming shortwave radiation (SW<sub>in</sub>, W m<sup>-2</sup>) in these regions (Kirtman *et al.*, 2013). In contrast, indirect climate change impacts result from changes in ecosystem composition, structure, and function

thus altering how ecosystems may respond to variations in meteorological conditions. For example, a gradual increase in the temperature sensitivity of ER over several years can alter NEE of boreal forests in the absence of any warming trend (e.g., Hadden & Grelle, 2016). The abrupt vegetation changes following permafrost thaw in lowland boreal forests may trigger shifts in ecosystem function (Camill *et al.*, 2001). Thus, both direct and indirect climate change effects on GPP and ER need to be assessed to better constrain the future NEE of organic-rich boreal landscapes in the permafrost zone.

Here, we examine the direct climate change effects of altered meteorological conditions and the indirect effects of thaw-induced wetland expansion on NEE and its component fluxes GPP and ER for a boreal forest-wetland landscape in a rapidly thawing lowland region at the southern limit of permafrost in northwestern Canada (Quinton *et al.*, 2011; Baltzer *et al.*, 2014).

We use nested eddy covariance net CO<sub>2</sub> flux measurements to compare NEE of the thawing landscape to NEE of a nearby permafrost-free wetland within the heterogeneous landscape, both exposed to the same meteorological conditions. Downscaled regional climate projections are used to assess the GPP, ER, and NEE response to a changing climate. We analyse

- (i) how thaw-induced wetland expansion and associated forest loss indirectly affect NEE, GPP, and ER of the boreal forest-wetland landscape, and
- (ii) how these indirect climate change effects compare to direct effects of projected changes in  $T_a$  and  $SW_{in}$  over the 21<sup>st</sup> century.

## Materials and Methods

### Study site

Scotty Creek (61°18' N; 121°18' W) is a 152-km<sup>2</sup> watershed in the sporadic permafrost zone (10-50% of land area underlain by permafrost) near Fort Simpson, NT in the southern Taiga Plains of northwestern Canada. With 70 Pg of soil organic C in the top 3 meters, the Taiga Plains store about 15 % of the total organic C stocks (<3 m) in the North American permafrost zone (data from Hugelius *et al.*, 2013). The dry continental climate of the Fort Simpson region is characterized by a mean T<sub>a</sub> of -2.8 °C and a mean total precipitation of 388 mm with 149 mm falling as snow (1981-2010; Environment Canada, 2014). The southern part of Scotty Creek is characterized by a mosaic of forested permafrost (peat) plateaus, wetlands, forested uplands and shallow lakes (Chasmer *et al.*, 2014). Permafrost-free wetlands (“wetlands”) occur mainly as collapse-scar bogs dominated by bryophytes (*Sphagnum balticum* and *S. magellanicum*), ericaceous shrubs (*Chamaedaphne calyculata*, *Andromeda polifolia*, *Vaccinium oxycoccos*), pod grass (*Scheuchzeria palustris*), and a few isolated black spruce (*Picea mariana*) and tamarack (*Larix laricina*). In contrast, forested permafrost plateaus (“forests”) are characterized by a denser overstorey of black spruce with a shrub understorey and a ground cover comprising ericaceous shrubs (mainly *Rhododendron groenlandicum*), and lichens (*Cladonia* spp.) and bryophytes (*Sphagnum fuscum* and *S. capillifolium*), respectively (Garon-Labrecque *et al.*, 2015). Abiotic and biotic characteristics change abruptly between these two ecosystem types as indicated by contrasting overstorey leaf area index ( $\geq 1$  vs.  $\leq 0.5$  for forest and wetland, respectively) and soil moisture conditions ( $\leq 30$  % for the forests compared to  $\geq 70$  % for the wetlands). An active layer (i.e., seasonally thawed surface soil) of approximately 50 cm overlays near-surface permafrost in the forests. No near-surface permafrost is present in the wetlands

(Baltzer *et al.*, 2014). These changes occur over several meters across transition zones with inundated, warmer peat soils (Bubier *et al.*, 1995; Baltzer *et al.*, 2014; Fig. 1). Warm soils in the wetlands cause lateral thawing of near-surface permafrost underlying the forests and, thus, a rapid expansion of permafrost-free wetlands (Kurylyk *et al.*, 2016). At Scotty Creek, forests and wetlands comprise thick organic peat soils of  $\geq 3$  m with a mean total organic C content of  $167 \pm 11$  kg C m<sup>-2</sup> ( $n = 3$ ; Pelletier *et al.*, in press). About 20 % of North America's boreal forests grow in the circumpolar permafrost zone on ice-rich permafrost and thick overburden cover, and are thus prone to thaw-induced surface subsidence and to forest loss in a warming climate (Helbig *et al.*, 2016a; Olefeldt *et al.*, 2016).

### **Eddy covariance measurements**

Eddy covariance net CO<sub>2</sub> flux measurements were conducted at a landscape tower at 15.2 m above the mean lichen-moss surface of the permafrost plateau (23 March 2015 to 30 August 2016) and at a nested wetland tower at 1.9 m above the mean moss surface (10 June 2015 to 30 August 2016). At the wetland and the landscape tower, high-frequency (10 Hz) fluctuations of vertical wind velocity and sonic temperature were measured with a sonic anemometer (CSAT3A, Campbell Scientific, Logan, UT) and CO<sub>2</sub> and water vapor densities with a co-located open-path infrared gas analyzer (EC150, Campbell Scientific). At the beginning of the study period (23 March 2015 to 16 August 2015), an enclosed infrared gas analyzer (LI-7200, LI-COR Biosciences, Lincoln, NE) was used for CO<sub>2</sub> and water vapor density measurements at the landscape tower. Differences in net CO<sub>2</sub> fluxes derived from the LI-7200 and the EC150 were less than 5 % and cumulative net CO<sub>2</sub> fluxes over 57 days differed by 8 % (Helbig *et al.*, 2016c). Net ecosystem CO<sub>2</sub> exchange for the landscape ( $NEE_{\text{LAND}}$ ;  $\mu\text{mol m}^{-2} \text{s}^{-1}$ ) and the wetland



tower ( $NEE_{WET}$ ;  $\mu\text{mol m}^{-2} \text{s}^{-1}$ ) was calculated as the sum of the turbulent net  $\text{CO}_2$  flux and a storage term. The storage term was derived from half-hourly  $\text{CO}_2$  concentration changes at the measurement heights. We follow the micrometeorological NEE convention where net landscape/ecosystem  $\text{CO}_2$  uptake is indicated by a negative sign and net  $\text{CO}_2$  release to the atmosphere by a positive sign. Net ecosystem  $\text{CO}_2$  exchange was filtered for periods with insufficient turbulence using a landscape tower friction velocity threshold of  $0.13 \text{ m s}^{-1}$  (95 % confidence interval (CI):  $0.10 - 0.21 \text{ m s}^{-1}$ ), derived according to Papale *et al.* (2006). The 95 % CI was derived by using 100 bootstrapped nighttime NEE time series as input. The same threshold was used for the wetland and the landscape tower as the wetland is nested in the landscape tower footprints (Fig. S1). All flux calculations were done using the EddyPro software (version 6.1.0, LI-COR Biosciences). A more detailed description of the instrumental setup and the flux processing procedure is given in Helbig *et al.* (2016b) and Helbig *et al.* (2016c). For the entire study period, 55 % (daytime: 68 %; nighttime: 39 %) and 43 % (daytime: 56 %; nighttime: 28 %) of NEE passed the quality control at the landscape and wetland tower, respectively.

## **Assessing indirect climate change impacts on $\text{CO}_2$ fluxes using nested eddy covariance fluxes**

### ***Footprint modeling***

Half-hourly 2-D flux footprints for the wetland and the landscape tower (defined as half-hourly probability maps of flux contribution per unit area [% per  $\text{m}^2$ ]) were obtained according to Kljun *et al.* (2015). The flux footprints were combined with a land cover classification map (Chasmer *et al.*, 2014), as described by Helbig *et al.* (2016b), to derive sums of half-hourly probabilities of flux contributions for individual land cover types (i.e., flux footprint

contributions from forests and wetlands; Fig. 1). Additionally, transition zones were delineated based on aerial photographs as areas of wetland expansion (and thus of forest loss) since 1977 (see Chasmer *et al.*, 2010). Within a radius of 350 m around the landscaper tower, 21 % of the land surface was classified as transition zone. Their flux footprint contributions were then separately derived for each half-hourly flux measurement. Transition zones are part of the wetland land cover type and their definition is to some extent arbitrary, as a reference year (here 1977, the first year of available aerial photography) is used to differentiate between gradual transition zones and interior wetlands. As the half-hourly variability in transition zone contribution was relatively small (standard deviation: 2 % for wetland tower and 5 % for landscape tower), only their average flux footprint contribution to the two flux towers over the entire study period was analyzed. Wetland NEE was discarded when forest contributions were greater than 5 % and  $NEE_{LAND}$  was discarded when contributions from a nearby lake were larger than 5 % (Fig. 1). On average, forest contributions to landscape tower footprints were 48 % whereas wetlands contributed 50 % (48 % from bogs and 2 % from fens). The remaining contributions originated from the nearby lake. The wetland tower was located in a collapse-scar bog and wetlands within the landscape tower footprint consisted to >95% of collapse-scar bogs. In the following, “wetlands” therefore refer to collapse-scar bogs. Fens represent a second permafrost-free wetland ecosystem type covering about 12% of the entire Scotty Creek watershed (Chasmer *et al.*, 2014). Similar to collapse-scar bogs, fens are expanding due to permafrost thaw (Chasmer & Hopkinson, in press). Due to their differing hydrology, vegetation composition, and nutrient availability, CO<sub>2</sub> flux dynamics of fens most likely differ from CO<sub>2</sub> flux dynamics of collapse-scar bogs (e.g.; Bubier, 1995; Yu, 2006; Treat *et al.*, 2016).

### Flux partitioning

Gaps in NEE were filled using the marginal distribution sampling method (Reichstein *et al.*, 2005) with  $SW_{in}$ ,  $T_a$ , and water vapor pressure deficit (VPD, kPa) as look-up table variables. We calculated annual NEE for 100 friction velocity thresholds (as derived from bootstrapped nighttime NEE) to derive the 95 % CI of annual NEE.

To partition NEE into its component fluxes, GPP ( $\mu\text{mol m}^{-2} \text{s}^{-1}$ ) and ER ( $\mu\text{mol m}^{-2} \text{s}^{-1}$ ), we used a bulk partitioning approach (e.g.; Runkle *et al.*, 2013). The non-gap-filled, half-hourly daytime NEE ( $SW_{in} > 5 \text{ W m}^{-2}$ ) was fit to a bulk model combining a rectangular hyperbola function (for GPP) and an empirical  $Q_{10}$  model (for ER):

$$NEE = -GPP + ER = -\underbrace{\frac{GPP_{max} \alpha SW_{in}}{GPP_{max} + \alpha SW_{in}}}_{\text{Term A}} + \underbrace{ER_{base} Q_{10}^{\frac{T_a - T_{ref}}{\gamma}}}_{\text{Term B}} \quad (1)$$

where  $GPP_{max}$  ( $\mu\text{mol m}^{-2} \text{s}^{-1}$ ) is the maximum canopy photosynthetic capacity,  $\alpha$  ( $\mu\text{mol m}^{-2} \text{s}^{-1}$  per  $\text{W m}^{-2}$ ) is the initial canopy quantum efficiency,  $ER_{base}$  ( $\mu\text{mol m}^{-2} \text{s}^{-1}$ ) is the basal respiration at a reference temperature ( $T_{ref} = 15 \text{ }^\circ\text{C}$ ),  $Q_{10}$  indicates the sensitivity of  $ER$  to  $T_a$ , and  $\gamma = 10 \text{ }^\circ\text{C}$  is a constant (e.g.; Mahecha *et al.*, 2010). For the  $Q_{10}$  model, we selected  $T_a$  measurements within the forest canopy at 2 m above the lichen-moss surface because  $T_a$  represents an integrated temperature measure for the landscape whereas soil temperature varies spatially (laterally and vertically) across the heterogeneous landscape (Helbig *et al.*, in press). We fixed the  $Q_{10}$  parameter in a first iteration ( $Q_{10} = 2.5$  [landscape] and  $Q_{10} = 1.1$  [wetland]) before deriving the final  $GPP_{max}$ ,  $\alpha$ , and  $ER_{base}$ , as described in Reichstein *et al.* (2005). To derive a complete  $ER$  time series, we combined gap-filled nighttime NEE (i.e.,  $ER$ ) with the modeled daytime  $ER$  (see Term B in Eqn. 1). Ecosystem respiration was then subtracted from measured NEE to derive GPP. By using only daytime NEE to obtain daytime  $ER$ , we account for

potential light inhibition of leaf respiration during the day (Wehr *et al.*, 2016) and avoid problems of extrapolating relationships between nighttime  $T_a$  and ER to daytime conditions (e.g., Lasslop *et al.*, 2010). We assessed indirect land cover change impacts on  $CO_2$  fluxes by analysing differences between NEE and derived component fluxes from the two eddy covariance flux towers with contrasting flux footprint composition.

### **Modeling NEE and GPP**

In this study, we assess how daily light- and temperature-conditions affect mean daily  $NEE_{LAND}$ . Net ecosystem  $CO_2$  exchange is the small difference between its two large component fluxes GPP and ER. Ecosystem respiration is strongly controlled by temperature whereas light and temperature are strong controls on GPP, highlighting the potentially different responses of ER and GPP to changing climatic conditions (e.g., Fang & Moncrieff, 2001; Huxman *et al.*, 2003; Lafleur *et al.*, 2005). We therefore modeled light-regulation of GPP using the rectangular hyperbola function in Eqn. 1 and used a downward regulation scalar [ $f(T_a)$  in Eqn. 2] to account for temperature-limitation of GPP. Mean daily GPP was fitted to the following equation with the *nlinfit* function in Matlab (version 8.6.0; The MathWorks, Natick, MA) using daily means of  $T_a$  and  $SW_{in}$ :

$$GPP = f(T_a) \times \frac{GPP_{max} \alpha SW_{in}}{GPP_{max} + \alpha SW_{in}} \quad (2)$$

$f(T_a)$  is implemented as a sigmoidal function ranging from 0 to 1 and accounts for instantaneous temperature constraints using mean daily  $T_a$  and for seasonal temperature constraints using a moving  $T_a$  average (i.e., average of seven preceding days,  $T_{a\_week}$ ; °C). The  $T_{a\_week}$  constraint accounts for seasonality in biological controls other than the instantaneous GPP response to  $T_a$ , such as physiological activity (e.g., Rayment *et al.*, 2002) and thermal

acclimation (e.g., Gea-Izquierdo *et al.*, 2010). According to Liebig's law, we assume that only the more limiting factor controls GPP (e.g.; Yuan *et al.*, 2007):

$$f(T_a) = \min \left( \frac{1}{1+a^{(b-T_a)}}, \frac{1}{1+a^{(c-T_{a\_week})}} \right) \quad (3)$$

where  $a$ ,  $b$ , and  $c$  are model coefficients. Additionally, we constructed an ER model (ER<sub>MOD</sub>) by fitting a  $Q_{10}$ -model (term B in Eqn. 1 based on daily  $T_a$ ) to mean daily ER. Modeled NEE (NEE<sub>MOD</sub>) was calculated as the sum of GPP<sub>MOD</sub> and ER<sub>MOD</sub>. Thus, NEE<sub>MOD</sub> only depends on the climatic controls  $T_a$  and SW<sub>in</sub> and does not account for other environmental or biological limitations on NEE (e.g.; soil moisture limitations; Niu *et al.*, 2011; Peichl *et al.*, 2013). Model uncertainties were estimated based on 1000 bootstrapped GPP and ER time series.

To characterize how the potential of NEE<sub>LAND</sub> (NEE<sub>POT</sub>) responds to changes in thermal conditions, we defined NEE<sub>POT</sub> as the most negative daily NEE<sub>LAND</sub> for given daily  $T_a$  (i.e., NEE<sub>LAND</sub> < 15 percentile per  $T_a$  bin with each bin containing 2.5 % of all data). Like NEE<sub>POT</sub>, we defined the temperature controlled potential of GPP<sub>LAND</sub> (GPP<sub>POT- $T_a$</sub> ) as the upper limit of daily GPP<sub>LAND</sub> for a given daily  $T_a$  and  $T_{a\_week}$ . To characterize the light control on the potential of GPP<sub>LAND</sub> (GPP<sub>POT-SW<sub>in</sub></sub>), we defined GPP<sub>POT-SW<sub>in</sub></sub> as the upper limit of daily GPP<sub>LAND</sub> for a given daily SW<sub>in</sub>. Sigmoidal functions were then fitted to GPP<sub>POT- $T_a$</sub>  and GPP<sub>POT-SW<sub>in</sub></sub>:

$$GPP_{POT-i} = \frac{k}{1+l^{(m-x_i)}} + n \quad (4)$$

where GPP<sub>POT- $i$</sub>  is modeled GPP<sub>POT</sub> for the variable  $x_i$  (i.e.,  $T_a/T_{a\_week}$  and SW<sub>in</sub>) and  $k$ ,  $m$ ,  $n$ , and  $l$  are model coefficients. We defined GPP<sub>POT</sub> as temperature-limited if GPP<sub>POT- $T_a$</sub>  for the observed daily  $T_a$  or  $T_{a\_week}$  was smaller than GPP<sub>POT-SW<sub>in</sub></sub> for the observed daily SW<sub>in</sub>. For the opposite case, GPP<sub>POT</sub> was light-limited. If differences in GPP<sub>POT- $T_a$</sub>  and GPP<sub>POT-SW<sub>in</sub></sub> were less than 10 %, we assumed that GPP<sub>POT</sub> was co-limited by temperature and light.

## Assessing direct climate change impacts on NEE

To assess direct climate change impacts on  $NEE_{MOD}$ ,  $GPP_{MOD}$ , and  $ER_{MOD}$ , we used the modelling approach described above with regionally downscaled climate projections as drivers. We obtained  $T_a$  and  $SW_{in}$  for the period 2006 to 2015 and 2091 to 2100 from the North American Coordinated Regional Climate Downscaling Experiment (CORDEX; <http://www.cordex.org>) and extracted daily time series for Scotty Creek. The CORDEX provides downscaled climate projections at 50-km resolution for various combinations of Earth system models (ESM) and regional climate models (RCM). We used the ensemble means of six CORDEX projections for two Representative Concentration Pathways (RCP) scenarios: the medium warming RCP4.5 and the high warming RCP8.5 scenario (for selected RCM/ESM simulations see Fig. S9; <https://na-cordex.org/simulations-modeling-group>). We used both RCPs to compare the scenario leading to the strongest warming (RCP8.5) with a more moderate scenario (RCP4.5). Currently, global net  $CO_2$  emissions follow the most pessimistic  $CO_2$  emission scenario, but these may potentially be reduced depending on future climate policies (Friedlingstein *et al.*, 2014a). To adjust for potential systematic differences between modeled (CORDEX) and measured  $T_a$ , we debiased modeled  $T_a$  for each CORDEX projection before calculating ensemble means by regressing it against measurements of daily  $T_a$  (Wilby *et al.*, 2004) from the nearest weather station in Fort Simpson (~50 km; 2006-2015; Environment Canada, 2016; [http://climate.weather.gc.ca/climate\\_data/](http://climate.weather.gc.ca/climate_data/)). We constrained the regression to periods when both CORDEX and weather station  $T_a > -5$  °C as the root-mean-square-error between modeled and measured  $T_a$  for colder periods increased by about 50 % (Fig. S5).

## Results

### Half-hourly landscape and wetland NEE

Between 10 June 2015 and 30 August 2016 wetlands and forests contributed equally to landscape flux footprints with  $50 \pm 30$  % ( $\pm 95$  % CI) and  $47 \pm 28$  %, respectively (and 3 % from the lake). About a third of the wetland contributions to the landscape flux footprints originated from the forest-to-wetland transition zones (i.e., total transition zone contributions to landscape flux footprints were  $18 \pm 10$  %). In contrast, transitions zones only contributed  $3 \pm 3$  % to the wetland flux footprints.  $NEE_{LAND}$  ranged from  $-7.9 \mu\text{mol m}^{-2} \text{s}^{-1}$  (1 %-ile) to  $4.8 \mu\text{mol m}^{-2} \text{s}^{-1}$  (99 %-ile) whereas a smaller range from  $-5.2 \mu\text{mol m}^{-2} \text{s}^{-1}$  (1 %-ile) to  $3.9 \mu\text{mol m}^{-2} \text{s}^{-1}$  (99 %-ile) was observed for  $NEE_{WET}$  (Fig. 2a). Positive  $NEE_{LAND}$  was more positive (i.e., more net  $\text{CO}_2$  release) than  $NEE_{WET}$  and negative  $NEE_{LAND}$  was more negative (i.e., more net  $\text{CO}_2$  uptake) than  $NEE_{WET}$  with a total least-squares (TLS) slope between  $NEE_{WET}$  and  $NEE_{LAND}$  of  $1.49 \pm 0.03$  and an intercept of  $0.24 \pm 0.03 \mu\text{mol m}^{-2} \text{s}^{-1}$ . Slopes for this relationship were independent of wetland contributions ( $FP_{WET}$ ; %) to landscape flux footprints. The slope for periods with  $FP_{WET}$  smaller than or equal to 50 % ( $1.50 \pm 0.05$ ) was not significantly different ( $\alpha = 0.05$ ) from the slope for periods with  $FP_{WET}$  larger than 50 % ( $1.43 \pm 0.03$ ). Slopes were consistently positive for night- and daytime  $NEE_{LAND}$  against  $NEE_{WET}$  relationships. However, the nighttime slope for low  $FP_{WET}$  ( $1.32 \pm 0.18$ ) was significantly smaller than the slope for high  $FP_{WET}$  ( $1.81 \pm 0.15$ ), indicating that nighttime  $NEE_{LAND}$  differed more from  $NEE_{WET}$  when wetland contributions to landscape flux footprints were large. For the daytime  $NEE_{WET}$  and  $NEE_{LAND}$  relationships, the slope for high  $FP_{WET}$  of  $1.52 \pm 0.05$  was significantly smaller than the slope for low  $FP_{WET}$  of  $1.71 \pm 0.07$ .  $NEE_{LAND}$  and  $NEE_{WET}$  relationships were independent of wind direction (Fig. S2) as

slopes for periods with northerly winds with overlapping wetland and landscape flux footprints were similar to slopes for periods with non-overlapping footprints (Fig. S2).

### **Daily landscape and wetland NEE and their component fluxes**

Monthly medians of daily  $NEE_{LAND}$  and  $NEE_{WET}$  were negative from May to August (i.e., net  $CO_2$  uptake period) when minimum daily  $T_a$  were generally warmer than  $0\text{ }^{\circ}C$  and positive for the remaining eight months with minimum daily  $T_a$  at or below  $0\text{ }^{\circ}C$  for most of the days (Fig. 3a, Fig. S3 & S4). Maximum positive daily  $NEE_{LAND}$  and  $NEE_{WET}$  were observed in November 2015 with medians of  $0.48\text{ }\mu\text{mol m}^{-2}\text{ s}^{-1}$  and  $0.46\text{ }\mu\text{mol m}^{-2}\text{ s}^{-1}$ , respectively, when  $T_a$  was below  $0\text{ }^{\circ}C$ , maximum  $SW_{in}$  smaller than  $200\text{ W m}^{-2}$ , but soil temperatures in the wetlands (at 32 cm) still between  $1\text{ }^{\circ}C$  and  $2.5\text{ }^{\circ}C$  (Fig. S4). Minimum negative  $NEE_{WET}$  and  $NEE_{LAND}$  in 2016 occurred in July with  $-0.86\text{ }\mu\text{mol m}^{-2}\text{ s}^{-1}$  and  $-1.01\text{ }\mu\text{mol m}^{-2}\text{ s}^{-1}$ , respectively. From May to July 2015 monthly medians of daily  $NEE_{LAND}$  were more negative than  $NEE_{WET}$  (Wilcoxon signed-rank test;  $p < 0.05$ ). In contrast, the median of daily  $NEE_{LAND}$  was less negative than  $NEE_{WET}$  in August 2015 (Wilcoxon signed-rank test;  $p < 0.001$ ) and not significantly different during the same month in 2016. Monthly medians of daily  $NEE_{LAND}$  in September, October, and December were more positive than  $NEE_{WET}$  while no significant differences were observed for the remaining winter months. Differences in the derived daily component fluxes GPP and ER were more pronounced with monthly medians of daily  $GPP_{WET}$  and  $ER_{WET}$  being significantly smaller than  $GPP_{LAND}$  and  $ER_{LAND}$  from March to November (Fig. 3 b & c). During the winter months between December and April, differences in landscape and wetland GPP and ER were smaller than  $0.1\text{ }\mu\text{mol m}^{-2}\text{ s}^{-1}$ . The largest GPP and ER differences were observed in June 2015 with monthly medians of  $GPP_{WET}$  being  $1.8\text{ }\mu\text{mol m}^{-2}\text{ s}^{-1}$  smaller than medians of  $GPP_{LAND}$  and



monthly medians of  $ER_{WET}$  being  $1.6 \mu\text{mol m}^{-2} \text{s}^{-1}$  smaller than medians of  $ER_{LAND}$ . In 2016, the largest differences in monthly medians of GPP and ER were observed in July with  $1.5 \mu\text{mol m}^{-2} \text{s}^{-1}$  and  $1.3 \mu\text{mol m}^{-2} \text{s}^{-1}$ , respectively. Between 2015 and 2016, the patterns and magnitude of NEE, GPP, and ER from both towers were similar for the overlapping months April to August.

### **Annual landscape and wetland NEE**

Annual cumulative  $NEE_{LAND}$  and  $NEE_{WET}$  ( $\Sigma NEE$ , g C-CO<sub>2</sub> m<sup>-2</sup>; 1 August 2015 to 31 July 2016) were not significantly different with  $-20.1 \text{ g C-CO}_2 \text{ m}^{-2}$  ( $-14.6$  to  $-26.9 \text{ g C-CO}_2 \text{ m}^{-2}$  [95 % CI]) and  $-23.5 \text{ g C-CO}_2 \text{ m}^{-2}$  ( $-19.6$  to  $-35.1 \text{ g C-CO}_2 \text{ m}^{-2}$ ), respectively (Fig. 4). Both the landscape and the wetland were thus small net CO<sub>2</sub> sinks. Shortly after snowmelt, the landscape and wetland wintertime net CO<sub>2</sub> source switched to a net CO<sub>2</sub> sink. From August 2015 until the end of snowmelt in 2016,  $\Sigma NEE_{LAND}$  was more positive ( $65.1 \text{ g C-CO}_2 \text{ m}^{-2}$ ) than  $\Sigma NEE_{WET}$  ( $39.3 \text{ g C-CO}_2 \text{ m}^{-2}$ ). The following larger landscape net CO<sub>2</sub> uptake between May and July 2016 reduced the annual  $\Sigma NEE$  differences to  $3.4 \text{ g C-CO}_2 \text{ m}^{-2}$ . Only in the beginning of January, wetland soil temperature (at 32 cm) dropped near the freezing temperature of water (Fig. S4) and the mean early winter (October to December) respiratory net CO<sub>2</sub> losses at the wetland and landscape tower dropped by more than 50 %, remaining low until snowmelt (January to April). In contrast to  $\Sigma NEE_{LAND}$  and  $\Sigma NEE_{WET}$ , the  $\Sigma GPP_{LAND}$  of  $532 \text{ g C-CO}_2 \text{ m}^{-2}$  was larger than the  $\Sigma GPP_{WET}$  of  $378 \text{ g C-CO}_2 \text{ m}^{-2}$ . Similarly, the  $\Sigma ER_{LAND}$  ( $512 \text{ g C-CO}_2 \text{ m}^{-2}$ ) exceeded the  $\Sigma ER_{WET}$  ( $355 \text{ g C-CO}_2 \text{ m}^{-2}$ , data not shown).

## Meteorological controls of potential NEE, GPP, and ER

While both  $GPP_{LAND}$  and  $ER_{LAND}$  increased consistently with  $T_a$ , the largest mean daily net  $CO_2$  uptake ( $NEE_{LAND}$ ) was observed at mean daily  $T_a$  of approximately 15 °C (Tab. 1 & Fig. 5). Daily mean  $NEE_{POT}$  was  $\sim 0 \mu mol m^{-2} s^{-1}$  for mean daily  $T_a < 2$  °C, became increasingly more negative at warmer  $T_a$  reaching a minimum of  $\sim -2 \mu mol m^{-2} s^{-1}$  at about 15 °C, before it became again slightly less negative for warmer  $T_a$  (Fig. 5a). Currently, mean daily  $T_a$  at Fort Simpson is below 2 °C on more than 50 % of the days of the year (median of 0.2 °C; 2006-2015). In contrast, only about 43 % of days are projected to be below this threshold at the end of the 21<sup>st</sup> century for the RCP 8.5 scenario (median of 4.8 °C; 2091-2100). Under the current climate, 15 % of daily  $T_a$  exceed the optimum  $NEE_{POT}$  temperature of 15 °C. The fraction of days with daily  $T_a$  above this threshold is projected to rise to 30 % (RCP8.5) by the end of the 21<sup>st</sup> century. Both  $T_a$  and  $SW_{in}$  limit  $GPP_{POT}$  (Fig. 5 b - d). Maximum mean daily  $GPP_{LAND}$  of  $\sim 6 \mu mol m^{-2} s^{-1}$  was observed when mean daily  $T_a$  and  $T_{a\_week}$  were warmer than 15 °C and mean daily  $SW_{in}$  was larger than  $\sim 200 W m^{-2}$ . Mean daily  $ER_{LAND}$  rapidly increased with  $T_a$  above the freezing point reaching a maximum  $ER_{LAND}$  of  $\sim 5 \mu mol m^{-2} s^{-1}$  at  $T_a$  warmer than 20 °C. The  $T_a$ -based  $Q_{10}$ -model explained 75 % of the variance in daily  $ER_{LAND}$  (root-mean-square error (RMSE):  $0.8 \mu mol m^{-2} s^{-1}$ ; for model parameters see Fig. 6 & Tab. S1). The combined  $T_a$ - $SW_{in}$  model of  $GPP_{LAND}$  explained 88 % of the variance in daily  $GPP_{LAND}$  (RMSE:  $0.7 \mu mol m^{-2} s^{-1}$ ; for model parameters see Tab. S1). Modeled  $NEE_{MOD}$  - the difference between  $GPP_{MOD}$  and  $ER_{MOD}$  - explained 45 % of the variance in mean daily  $NEE_{LAND}$  (RMSE:  $0.7 \mu mol m^{-2} s^{-1}$ ).

### Temperature- and light-limitation of GPP<sub>POT</sub>

During the measurement period, GPP<sub>POT</sub> was mainly temperature-limited in late winter (until early May) with cold  $T_a$  suppressing GPP despite high  $SW_{in}$  (Fig. 5 d & Fig. 7 a). With warming  $T_a$  in June 2016, the fraction of days when GPP<sub>POT</sub> was  $T_a$ -limited dropped to 33 % compared to 94 % in May 2016 (Fig. 7a). In July 2016, GPP<sub>POT</sub> was co-limited by  $T_a$  and  $SW_{in}$  on 74 % of days (Fig. 7b). Light-limitation of GPP was rare until July ( $\leq 10$  % of days) and became more frequent in August and October with 19 % and 23 % of days, respectively (Fig. 7c). From July to September, the fraction of days with  $T_a$ -limited GPP increased again from 13 % to 87 %.

Until the end of the 21<sup>st</sup> century (2091-2100), mean daily  $T_a$  between April and September at Scotty Creek is projected to increase by 2.5 °C for the RCP 4.5 or by 5.2 °C for the RCP 8.5 scenario compared to the period 2006 to 2015 (Fig. S6a-d). In contrast, mean daily  $SW_{in}$  for the same period is projected to decrease by 3 W m<sup>-2</sup> (RCP 4.5) and by 6.6 W m<sup>-2</sup> (RCP 8.5), most likely due to increased cloudiness as indicated by concurrent increases in precipitation (Fig. S6 e-l). These projected changes consistently reduce  $T_a$ -limitation of GPP<sub>POT</sub> between April and October. The largest reduction in the fraction of days with  $T_a$ -limited GPP<sub>POT</sub> is expected in June and September with -26 % and -22 % for the RCP 4.5 scenario and with -45 % and -47 % for the RCP 8.5 scenario, respectively. The largest increase in days with co-limited GPP<sub>POT</sub> is projected for June (+24 % [RCP 4.5] and +40 % [RCP 8.5]). Increases in the fraction of days with  $SW_{in}$ -limited GPP<sub>POT</sub> are most pronounced in September with 14 % (RCP 4.5) and 37 % (RCP 8.5). Between March and July, projected increases in days with  $SW_{in}$ -limited GPP<sub>POT</sub> are smaller than 10 % (RCP 4.5 and RCP 8.5).

### **Projected changes in $GPP_{MOD}$ , $ER_{MOD}$ , and $NEE_{MOD}$**

By the end of the 21<sup>st</sup> century, the projected changes in  $T_a$  and  $SW_{in}$  enhance  $GPP_{MOD}$  with maximum increases in May (Fig. 8). For the RCP 8.5 scenario, the projected increase in annual  $GPP_{MOD}$  is about twice as large as for the RCP 4.5 scenario. However, the increase in annual  $ER_{MOD}$  for the RCP 8.5 scenario is 2.5 times larger than for the RCP 4.5 scenario due to warmer  $T_a$ . In contrast to  $GPP_{MOD}$ , monthly  $ER_{MOD}$  is expected to increase most strongly in August and July. The differences in the timing of increases in  $GPP_{MOD}$  and  $ER_{MOD}$  result in a more negative  $NEE_{MOD}$  early in the summer and less negative  $NEE_{MOD}$  in July - the warmest summer month. Annual  $NEE_{MOD}$  switches its sign from  $-9 \pm 39$  g C-CO<sub>2</sub> m<sup>-2</sup> ( $\pm 95$  % CI; 2006-2015) to  $+16 \pm 42$  g C-CO<sub>2</sub> m<sup>-2</sup> (2091-2100) for the RCP 4.5 scenario and becomes a significant net CO<sub>2</sub> source with  $+94 \pm 54$  g C-CO<sub>2</sub> m<sup>-2</sup> (2091-2100) for the RCP 8.5 scenario. Similar annual  $NEE_{MOD}$  for the wetland (i.e.,  $NEE_{MOD}$  derived from  $GPP_{WET}$  and  $ER_{WET}$ ) was modeled with projected annual  $NEE_{MOD}$  (2091-2100) of  $-9 \pm 27$  g C-CO<sub>2</sub> m<sup>-2</sup> and  $+60 \pm 31$  g C-CO<sub>2</sub> m<sup>-2</sup> for the RCP 4.5 and the RCP 8.5 scenario, respectively (Fig. S7). While climatic changes both in winter and summer contribute to this change in annual  $NEE_{MOD}$ , the bulk of the reduction occurs during the summer months (May to September) for the RCP 8.5 scenario (73 %). For the RCP 4.5 scenario, an equal reduction occurs during the cold (October to April) and warm season (May to September).

### **Discussion**

#### **Indirect thaw-induced climate change impact on carbon dioxide fluxes**

At Scotty Creek, both half-hourly net CO<sub>2</sub> uptake during the day and net CO<sub>2</sub> release during the night were larger for the boreal forest-wetland landscape compared to the wetland (Fig. 2). However, half-hourly  $NEE_{LAND}$  differed more from  $NEE_{WET}$  with increasing wetland

contributions to landscape flux footprints. In contrast, sensible and latent heat (Helbig *et al.*, 2016b) and methane fluxes (Helbig *et al.*, in press) were found to scale with wetland contributions at Scotty Creek. An analysis of mean flux footprint contributions from forest-wetland transition zones revealed that these contributions were about six times larger for landscape than for wetland tower flux footprints (Fig. 1 c). The transition zones with higher soil moisture and warmer soil temperatures (Bubier *et al.*, 1995; Baltzer *et al.*, 2014) may be characterized by larger GPP and ER compared to the interior of the wetlands and the forests, both characterized by drier surface soils. Such spatial patterns of GPP and ER have previously been observed in similar permafrost peatlands using chamber methods (Turetsky *et al.*, 2002; Wickland *et al.*, 2006; Myers-Smith *et al.*, 2007). Methane fluxes may be more uniform across the wetland as these are more sensitive to variations in water table position compared to variations in surface soil moisture (e.g., Bubier *et al.*, 1995; Kettunen, 2003). In contrast, the productivity of the dominant plant genus in the wetland, *Sphagnum* spp., is strongly controlled by surface moisture (e.g., Schipperges & Rydin, 1998), potentially explaining the differing spatial patterns of NEE and methane fluxes.

Similar findings were reported for a thawing tundra landscape, where both GPP and ER of actively thawing patches within the landscape were larger than the integrated landscape GPP and ER (Belshe *et al.*, 2012). Permafrost thaw increases the availability of nitrogen (Finger *et al.*, 2016), increases surface soil moisture, and induces vegetation shifts toward more aquatic species (Camill, 1999; Camill *et al.*, 2001), potentially enhancing both productivity and respiration in the transition zones. Compared to the permafrost-free wetland, the larger extent of actively thawing transition zones in the boreal forest-wetland landscape may therefore cause larger  $GPP_{LAND}$  and  $ER_{LAND}$  (Fig. 2).

In contrast to  $\Sigma\text{GPP}$  and  $\Sigma\text{ER}$ , annual  $\Sigma\text{NEE}_{\text{LAND}}$  and  $\Sigma\text{NEE}_{\text{WET}}$  did not differ significantly at Scotty Creek (Fig. 3), suggesting that thaw-induced wetland expansion and forest loss might have a negligible short-term impact on  $\Sigma\text{NEE}$ . The long-term negative  $\Sigma\text{NEE}$  (i.e., net  $\text{CO}_2$  uptake) is a major component of peatland C budgets in addition to the typical C losses due to methane emissions and due to net lateral export of dissolved organic C (e.g.; Roulet *et al.*, 2007). At Scotty Creek, wetlands emit  $12 \text{ g C-CH}_4 \text{ m}^{-2}$  per year as opposed to  $6 \text{ g C-CH}_4 \text{ m}^{-2}$  at the landscape level (Helbig *et al.*, in press), suggesting a similar wetland and landscape net C uptake of  $-12 \text{ g C m}^{-2} \text{ yr}^{-1}$  ( $-24 \text{ g C-CO}_2 \text{ m}^{-2} + 12 \text{ g C-CH}_4 \text{ m}^{-2}$ ) and  $-14 \text{ g C m}^{-2} \text{ yr}^{-1}$  ( $-20 \text{ g C-CO}_2 \text{ m}^{-2} + 6 \text{ g C-CH}_4 \text{ m}^{-2}$ ), respectively (excluding lateral export of dissolved organic C [DOC]). For a boreal peatland landscape in the discontinuous permafrost zone of Manitoba, Moore (2003) reports small annual DOC exports between  $1.7$  and  $3.2 \text{ g C m}^{-2} \text{ yr}^{-1}$ . If DOC exports at Scotty Creek are of a similar magnitude, a current net C uptake of approximately  $10 \text{ g C m}^{-2} \text{ yr}^{-1}$  can be expected. A multi-site synthesis study reports similar long-term C accumulation rates for boreal permafrost peatlands [ $14 \text{ g C m}^{-2} \text{ yr}^{-1}$ ] and for permafrost-free bogs [ $18 \text{ g C m}^{-2} \text{ yr}^{-1}$ ] (Treat *et al.*, 2016). Similarly, growing-season NEE was not significantly different across a thaw chronosequence from a forested permafrost peat plateau to a collapse-scar bog in Alaska (Johnston *et al.*, 2014). For a permafrost peatland landscape in northern Manitoba, aboveground net primary productivity of permafrost peat plateaus and of collapse-scar bogs was similar, but a twofold increase in the accumulation of peat was observed following thaw (Camill *et al.*, 2001). Post-thaw increases in C accumulation have been reported for several thawing permafrost peatlands in Manitoba, Saskatchewan, Alberta, and Alaska (Camill, 1999; Turetsky *et al.*, 2000; Turetsky *et al.*, 2007; Jones *et al.*, 2013). However, enhanced decomposition of thawed forest peat has also been shown to exceed increased C accumulation rates in near-surface collapse-scar

bog peat, inducing a rapid post-thaw net C loss (O'Donnell *et al.*, 2012). Particularly transition zones may be subject to rapid net C losses, before they slowly return to a net C sink after about a decade (Jones *et al.*, 2016). Our findings suggest that thawing boreal forest-wetland landscapes can still act as net CO<sub>2</sub> sinks – and most likely as net C sinks - under the current climate. The continuing net CO<sub>2</sub> sink may be the result of integrating large areas with small net CO<sub>2</sub> uptake (e.g., forested permafrost plateaus and interior of permafrost-free wetlands) and small areas with potentially large net CO<sub>2</sub> loss (e.g., recently thawed transition zones). While the thaw-induced wetland expansion may affect long-term C cycle dynamics through its effect on regional hydrology (Connon *et al.*, 2014), species-specific productivity (Camill *et al.*, 2001), and fire regimes (Camill *et al.*, 2009), the immediate indirect climate warming impact of such land cover change on landscape NEE appears to be small.

### **Direct climate change impacts on carbon dioxide fluxes**

In contrast to the small indirect thaw-induced climate change impact on NEE, direct climate change effects appear to be larger and may depend strongly on the future CO<sub>2</sub> emission trajectories as represented by RCPs (Fig. 8). At Scotty Creek, early summer NEE<sub>MOD</sub> increases with warming T<sub>a</sub>, but decreases later in the summer. Such a seasonal pattern is supported by multi-year observations of NEE at other northern and alpine ecosystems (Huxman *et al.*, 2003; Piao *et al.*, 2008). Mid-summer GPP is often light-saturated and warmer summer T<sub>a</sub> only marginally enhances plant productivity. ER is mainly temperature-limited (in the absence of moisture stress) and warmer mid-summer T<sub>a</sub> reduces NEE by enhancing ER (Huxman *et al.*, 2003). In a warmer climate with more hot summer days (Fig. 5a), this increase in ER may eventually exceed GPP (Runkle *et al.*, 2013). At the tree level, increased white spruce tree-ring

growth in Alaska has been related to warmer spring temperatures for some individuals but also to decreased growth in response to warmer summer temperatures for other individuals (Wilmking *et al.*, 2004). Similar to this study, recent tree-ring and modelling analyses highlight the negative impacts of warmer summer  $T_a$  - and an associated increase in autotrophic respiration - on net primary productivity (i.e., balance between GPP and autotrophic respiration) of black spruce forests (Girardin *et al.*, 2016). Additionally, warmer summer  $T_a$  may accelerate evapotranspiration rates, decrease moisture availability, and enhance atmospheric water demand potentially slowing down GPP and/or ER during peak growing season (e.g.; Barber *et al.*, 2000; Kljun *et al.*, 2007; Novick *et al.*, 2016).

In fall, light-limitation of GPP is more frequent than in spring (Niu *et al.*, 2011; Fig. 7), potentially explaining the larger spring response in  $GPP_{MOD}$  to warmer  $T_a$ . For a subalpine forest, Huxman *et al.* (2003) found two NEE minima in early and late summer with a reduction in net  $CO_2$  uptake in mid-summer. Here, we observed only one NEE minimum in July for the current seasonal NEE pattern at Scotty Creek. However, similar to Huxman *et al.* (2003), projected  $NEE_{MOD}$  is characterised by two minima in June and August for the RCP 4.5 scenario. In the RCP 8.5 scenario, the  $NEE_{MOD}$  minima in early and late summer are even more pronounced (Fig. 8).

In a recent modeling synthesis study, McGuire *et al.* (2016) found that moderate warming in the northern circumpolar permafrost region increased GPP, and vegetation C stocks, but decreased soil C stocks over a 50-year time period in most ESMs. Atmospheric inversion models indicate an increasing net  $CO_2$  sink in the boreal biome for the period 1985 to 2012 (Welp *et al.*, 2016; 50° - 60° N). These results are supported by site-level NEE measurements for temperate and boreal forests indicating that earlier spring onset (i.e., warmer  $T_a$ ) consistently increases



GPP, and to a lesser extent ER (Kljun *et al.*, 2007; Richardson *et al.*, 2009; Richardson *et al.*, 2010). However, the positive productivity response of evergreen coniferous forests appears to be smaller compared to deciduous forests (Kljun *et al.*, 2007; Welp *et al.*, 2007; Richardson *et al.*, 2010). In a boreal forest ecosystem in the sporadic permafrost zone, longer growing seasons did not increase net CO<sub>2</sub> uptake as the positive productivity response was offset by enhanced respiration (Dunn *et al.*, 2007). In a boreal forest warming experiment, bud burst of black spruce trees occurred earlier and greater shoot lengths were observed (Bronson *et al.*, 2009). The increase in photosynthetic tissue may therefore enhance aboveground net primary productivity, even in the absence of changes in light-saturated photosynthesis and foliage respiration per m<sup>2</sup> of foliage (Bronson & Gower, 2010). Concurrent observations of decreases in fine root net primary productivity may, however, result in unchanged total net primary productivity (Bronson *et al.*, 2008).

Availability of organic C in permafrost peatland landscapes, such as Scotty Creek, is not limited (Treat *et al.*, 2016). Warmer T<sub>a</sub> may therefore gradually increase ER while the dominant temperature-limitation of GPP may switch to a more dominant light-limitation, limiting the productivity benefits of warming T<sub>a</sub> (Fig. 6 and 7). Air temperature effects on ER have been shown to exert a strong control on interannual variation of boreal forest NEE, exceeding the impacts of variations in GPP (Ueyama *et al.*, 2009; Ueyama *et al.*, 2014). In boreal forests, the NEE response to T<sub>a</sub> often follows a parabolic curve with a temperature-optimum of NEE followed by decreasing net CO<sub>2</sub> uptake with T<sub>a</sub> above this threshold (Grant *et al.*, 2009; Niu *et al.*, 2011; Fig. 6a). At Scotty Creek, this T<sub>a</sub>-threshold appears to be approximately 15 °C, slightly warmer than the 11-year mean NEE T<sub>a</sub>-optimum of 11±2 °C (± one standard deviation) for a boreal forest in the sporadic permafrost zone of northern Manitoba (Niu *et al.*, 2012). It should

be noted that, in the long-term, the NEE temperature-optimum might change with thermal adaptation of the vegetation or species composition shifts (Yuan *et al.*, 2011). In a warmer climate, the  $T_a$ -optimum of NEE in boreal landscapes like Scotty Creek is likely to be exceeded more often during the summer (Fig. 5a), potentially decreasing summertime net  $CO_2$  uptake. Our results suggest that, with continuously rising  $T_a$ , increases in net  $CO_2$  uptake of boreal forest-wetland landscapes may therefore eventually slow down, and their long-term net  $CO_2$  uptake may potentially decrease depending on the climate-warming scenario.

A decreasing potential of boreal forest-wetland landscapes to sequester  $CO_2$  in a warmer climate is supported by a projected C loss at the southern edge of the boreal biome where ecosystems with low potential for long-term C accumulation are expected to replace current boreal organic C-rich ecosystems (Koven, 2013). A diminishing potential net  $CO_2$  uptake may “push” the current C-accumulating landscapes to an unstable state increasing the potential for an abrupt transition to landscapes with lower C stocks and a loss of their  $CO_2$  sink function (Scheffer *et al.*, 2012). For the RCP4.5 scenario, current climates (i.e., mean annual  $T_a$  and total precipitation) similar to the projected end-of-the-century climate of Scotty Creek are found within the boreal biome in northern Alberta. For the RCP8.5 scenario, similar climates are currently found at the limit or south of the boreal biome in Canada and the northwestern United States (Fig. 9 and Fig. S8). In contrast to changes in  $T_a$  and precipitation,  $SW_{in}$  is more strongly bound to latitude. The limited duration of the period providing sufficient light for photosynthetic  $CO_2$  uptake combined with warmer  $T_a$  and more precipitation (Fig. S6) is therefore likely to increase ER more than GPP, particularly for the RCP8.5 scenario (Fig. 8). A shift from permafrost peatland landscapes with large organic C stocks (mean of  $106 \text{ kg m}^{-2} \pm 45$  [ $\pm$  one standard deviation] for forested permafrost plateaus [ $n = 158$ ];  $117 \text{ kg m}^{-2} \pm 65$  for collapse-scar

bogs [ $n = 52$ ]; data from Treat *et al.*, 2016) to landscapes with low C stocks would result in large net CO<sub>2</sub> emissions. Our results suggest that the magnitude of these emissions will strongly depend on future anthropogenic CO<sub>2</sub> emission pathways (Fig. 8).

### Comparison with Earth system models and CO<sub>2</sub> flux inversion modeling

A comparison with five end-of-21<sup>st</sup>-century ESM projections of NEE (from the Coupled Model Intercomparison Project [CMIP5; <http://cmip-pcmdi.llnl.gov/cmip5/>]; Friedlingstein *et al.*, 2014b; Fig. S9) shows that three out of five ESMs project NEE changes similar to our findings. More specifically, for the southern Taiga Plains region, no ESM shows significant changes in mean annual NEE for the moderate RCP4.5 scenario (Two-Sample *t*-test;  $\alpha = 0.05$ ;  $n = 10$ ). For the warmer RCP8.5 scenario, three out of the five ESMs indicate decreases in net CO<sub>2</sub> uptake (7 to 36 g C-CO<sub>2</sub> m<sup>-2</sup> less negative NEE with one ESM showing a significant decrease;  $p = 0.04$ ;  $n = 10$ ; see Fig. S9). Two ESMs even indicate a switch from a net CO<sub>2</sub> sink to a net CO<sub>2</sub> source. Similar to our study, all ESMs project the largest monthly increase in net CO<sub>2</sub> uptake between April and June (except for July in the RCP8.5 scenario of one ESM) and smaller increases or even decreases in net CO<sub>2</sub> uptake later in summer.

For the period 2006 to 2015, all five ESMs indicate a mean net CO<sub>2</sub> sink for the southern Taiga Plains region with differences of less than 20 g C-CO<sub>2</sub> m<sup>-2</sup> to measured annual NEE at Scotty Creek (except for a larger difference for one ESM; Fig. S10). Compared to the annual landscape NEE of -20 g C-CO<sub>2</sub> m<sup>-2</sup> at Scotty Creek, global CO<sub>2</sub> flux inversions (1° x 1° resolution, CarbonTracker, 2016) suggest a mean annual NEE (2006 – 2015) of -39±52 g C-CO<sub>2</sub> m<sup>-2</sup> [ $\pm$  one standard deviation] with a similar monthly NEE seasonality and magnitude (Fig. S10a). However, four out of five ESMs overestimate the maximum monthly net CO<sub>2</sub> uptake in

the summer and the maximum monthly net CO<sub>2</sub> loss in the winter. The ESMs simulate both direct and indirect climate change effects on NEE, but their NEE response may vary due to differing representations of land surface processes (e.g., dynamic vegetation models, phenology, CO<sub>2</sub> fertilization, nutrient dynamics) (e.g., Friedlingstein *et al.*, 2014b; Wieder *et al.*, 2015). Disentangling the individual contributions from these processes to diverging NEE projections is difficult due to the complex interactions between the individual model components (e.g., Friedlingstein *et al.*, 2014b). However, an improved understanding of temperature- and light-limitation of NEE may help reducing the wide spread in modeled boreal landscape NEE response to climate change and minimize the deviation between measured and modeled seasonality of NEE.

### **Potential responses of ecosystem functioning to a changing climate**

How vegetation productivity and respiration respond to changes in temperature and light may be affected by factors other than shifts in landscape and ecosystem composition and structure. Rising atmospheric CO<sub>2</sub> concentrations and the related fertilization effect on plant productivity may stimulate and enhance GPP (McGuire *et al.*, 2016). This CO<sub>2</sub> fertilization effect could directly increase GPP through its positive impact on maximum GPP (Ueyama *et al.*, 2016), favoring a larger potential for net CO<sub>2</sub> uptake than projected in this study. However, the magnitude of the CO<sub>2</sub> fertilization effect in boreal forests remains poorly constrained: both no productivity response (Kroner & Way, 2016) and a positive response was observed (Tjoelker *et al.*, 1998) in CO<sub>2</sub> fertilization experiments of Norway spruce (*Picea abies*) and black spruce seedlings. A small, positive GPP response of 0.16 % ppm<sup>-1</sup> (2002-2014) was estimated for an Alaskan black spruce forest (Ueyama *et al.*, 2016). Net primary productivity of about half of the

black spruce forests in North America (south of 60° N) was projected to decline at the end of the 21<sup>st</sup> century in a modeling study despite a positive CO<sub>2</sub> fertilization effect on GPP (Girardin *et al.*, 2016). For *Sphagnum* spp. and vascular bog species, only small or negative CO<sub>2</sub> effects on productivity were reported (Berendse *et al.*, 2001; Heijmans *et al.*, 2002). To some extent, plants can acclimate to warmer T<sub>a</sub> by modifying their photosynthetic and respiratory apparatus. In warming and CO<sub>2</sub> enrichment experiments, the thermal optimum of light-saturated net CO<sub>2</sub> uptake of both Norway spruce and black spruce seedlings increased in the warming treatments while leaf respiration was suppressed. At the same time, light-saturated net CO<sub>2</sub> uptake was found to decrease for the warmest treatments (+8 °C) (Way & Sage, 2008; Kroner & Way, 2016). A better constraint of the impacts of CO<sub>2</sub> fertilization and thermal acclimation on the productivity of boreal plant species is therefore needed to fully understand the response of boreal forest-wetland landscape CO<sub>2</sub> fluxes to climate change.

Our focus on meteorological controls (temperature and light) of GPP only constrains the GPP<sub>MOD</sub> response given no other limiting factors. Actual GPP however may be reduced by additional environmental limitations. For example, earlier spring onset in the boreal and temperate forests has been observed to decrease peak summer productivity due to soil moisture deficits later in the summer (Buermann *et al.*, 2013; Wolf *et al.*, 2016). Particularly in late summer and fall, soil moisture deficits can add another environmental constraint on GPP (Niu *et al.*, 2011). In peatlands, fluctuating water levels may also modify the temperature-sensitivity of heterotrophic soil respiration (e.g., Silvola *et al.*, 1996; Hanis *et al.*, 2015) and affect GPP (e.g., Chivers *et al.*, 2009). Changes in net primary productivity may alter C substrate availability to soil microbes through changes in litter fall (Bond-Lamberty *et al.*, 2004; Beier *et al.*, 2008) and changes in GPP may affect autotrophic respiration through the allocation of photosynthates

(Janssens *et al.*, 2001). Such indirect effects of ecosystem acclimation may modify the overall temperature sensitivity of ER and, therefore, additionally affect NEE responses to a changing climate. The temperature-response of ER in a warmer climate could also be attenuated if increasing net C losses diminish the fraction of labile organic C, exposing more recalcitrant organic matter from deeper peat layers, or induce temperature-related changes in soil microbial communities (Hogg *et al.*, 1992; Bradford *et al.*, 2008). Understanding how these environmental controls interact with the warming-related shifts in the seasonality of GPP and ER will help constraining the NEE response to a warmer climate.

Here, we show that thaw-induced wetland expansion and associated boreal forest loss appears to have negligible indirect climate change effects on the observed landscape net CO<sub>2</sub> uptake of ~20 g C-CO<sub>2</sub> m<sup>-2</sup> yr<sup>-1</sup>. However, even without moisture stress, net CO<sub>2</sub> uptake of boreal forest-wetland landscapes is likely to decline by the end of the 21<sup>st</sup> century due to direct climate change impacts of changing meteorological forcing. This projected reduction is about five times larger for a high climate-warming scenario (103 g C-CO<sub>2</sub> m<sup>-2</sup> yr<sup>-1</sup>) compared to a moderate scenario (25 g C-CO<sub>2</sub> m<sup>-2</sup> yr<sup>-1</sup>). In an exceedingly warmer climate, the recently observed increasing net CO<sub>2</sub> uptake of the boreal biome may therefore turn into a decreasing net CO<sub>2</sub> sink during the 21<sup>st</sup> century, reducing the ability of boreal landscapes to sequester atmospheric CO<sub>2</sub>.

## Acknowledgements

We thank three anonymous reviewers for their critical and constructive comments. MH was funded through graduate student scholarships provided by the Fonds de recherche du Québec – Nature et technologies (FRQNT) and the German Academic Exchange Service (DAAD). Funding for this research was awarded to OS by the Canada Research Chairs, Canada Foundation for Innovation Leaders Opportunity Fund and Natural Sciences and Engineering Research Council Discovery Grant programs. ARD acknowledges support from the U.S. Dept of Energy Lawrence Berkeley Lab Ameriflux Network Management Project. MH is thankful to Tanja Živković, Avni Malhotra, and Christoforos Pappas for discussions improving an earlier version of the manuscript. We are grateful for the support of the Liidlii Kue First Nation and Jean-Marie River First Nation for their support of the Scotty Creek Research Station. This study was part of the Arctic Boreal Vulnerability Experiment (ABoVE).

## References

- Baltzer JL, Veness T, Chasmer LE, Sniderhan AE, Quinton WL (2014) Forests on thawing permafrost: fragmentation, edge effects, and net forest loss. *Global Change Biology*, **20**, 824–834.
- Barber VA, Juday GP, Finney BP (2000) Reduced growth of Alaskan white spruce in the twentieth century from temperature-induced drought stress. *Nature*, **405**, 668–673.
- Beier C, Emmett BA, Peñuelas J et al. (2008) Carbon and nitrogen cycles in European ecosystems respond differently to global warming. *Science of the Total Environment*, **407**, 692–697.
- Belshe EF, Schuur EAG, Bolker BM, Bracho R (2012) Incorporating spatial heterogeneity created by permafrost thaw into a landscape carbon estimate. *Journal of Geophysical Research: Biogeosciences*, **117**, G01026.
- Berendse F, Van Breemen N, Rydin Ha et al. (2001) Raised atmospheric CO<sub>2</sub> levels and increased N deposition cause shifts in plant species composition and production in Sphagnum bogs. *Global Change Biology*, **7**, 591–598.
- Bond-Lamberty B, Wang C, Gower ST (2004) A global relationship between the heterotrophic and autotrophic components of soil respiration? *Global Change Biology*, **10**, 1756–1766.

- Bradford MA, Davies CA, Frey SD et al. (2008) Thermal adaptation of soil microbial respiration to elevated temperature. *Ecology Letters*, **11**, 1316–1327.
- Brandt JP (2009) The extent of the North American boreal zone. *Environmental Reviews*, **17**, 101–161.
- Bronson DR, Gower ST (2010) Ecosystem warming does not affect photosynthesis or aboveground autotrophic respiration for boreal black spruce. *Tree Physiology*, **30**, 441–449.
- Bronson D, Gower ST, Tanner M, Linder S, Van Herk I (2008) Response of soil surface CO<sub>2</sub> flux in a boreal forest to ecosystem warming. *Global Change Biology*, **14**, 856–867.
- Bronson DR, Gower ST, Tanner M, Van Herk I (2009) Effect of ecosystem warming on boreal black spruce bud burst and shoot growth. *Global Change Biology*, **15**, 1534–1543.
- Bubier JL (1995) The relationship of vegetation to methane emission and hydrochemical gradients in northern peatlands. *Journal of Ecology*, **83**, 403–420.
- Bubier JL, Moore TR, Bellisario L, Comer NT, Crill M (1995) Ecological controls on methane emissions from a northern peatland complex in the zone of discontinuous permafrost, Manitoba, Canada. *Global Biogeochemical Cycles*, **9**, 455–470.
- Buermann W, Bikash PR, Jung M, Burn DH, Reichstein M (2013) Earlier springs decrease peak summer productivity in North American boreal forests. *Environmental Research Letters*, **8**, 24027.
- Camill P (1999) Peat accumulation and succession following permafrost thaw in the boreal peatlands of Manitoba, Canada. *Écoscience*, **6**, 592–602.
- Camill P, Lynch JA, Clark JS, Adams JB, Jordan B (2001) Changes in biomass, aboveground net primary production, and peat accumulation following permafrost thaw in the boreal peatlands of Manitoba, Canada. *Ecosystems*, **4**, 461–478.
- Camill P, Barry A, Williams E, Andreassi C, Limmer J, Solick D (2009) Climate-vegetation-fire interactions and their impact on long-term carbon dynamics in a boreal peatland landscape in northern Manitoba, Canada. *Journal of Geophysical Research*, **114**, G04017.
- Chapin FS, McGuire AD, Randerson J et al. (2000) Arctic and boreal ecosystems of western North America as components of the climate system. *Global Change Biology*, **6**, 211–223.
- Chasmer LE, Hopkinson C, Quinton W (2010) Quantifying errors in discontinuous permafrost plateau change from optical data, Northwest Territories, Canada: 1947–2008. *Canadian Journal of Remote Sensing*, **36**, S211–S223.
- Chasmer LE, Hopkinson C, Veness T, Quinton W, Baltzer J (2014) A decision-tree classification for low-lying complex land cover types within the zone of discontinuous permafrost. *Remote Sensing of Environment*, **143**, 73–84.
- Chasmer LE, Hopkinson C (in press) Threshold Loss of Discontinuous Permafrost and Landscape Evolution. *Global Change Biology*, doi: 10.1111/gcb.13537.
- Chivers MR, Turetsky MR, Waddington JM, Harden JW, McGuire AD (2009) Effects of experimental water table and temperature manipulations on ecosystem CO<sub>2</sub> fluxes in an Alaskan rich fen. *Ecosystems*, **12**, 1329–1342.
- Connon RF, Quinton WL, Craig JR, Hayashi M (2014) Changing hydrologic connectivity due to permafrost thaw in the lower Liard River valley, NWT, Canada. *Hydrological Processes*,



28, 4163–4178.

- DeBeer CM, Wheeler HS, Carey SK, Chun KP (2016) Recent climatic, cryospheric, and hydrological changes over the interior of western Canada: a synthesis and review. *Hydrology and Earth System Sciences*, **20**, 1573–1598.
- Dunn AL, Barford CC, Wofsy SC, Goulden ML, Daube BC (2007) A long-term record of carbon exchange in a boreal black spruce forest: means, responses to interannual variability, and decadal trends. *Global Change Biology*, **13**, 577–590.
- Environment Canada (2014) Canadian Climate Normals: 1981 - 2010. Available at: [http://climate.weather.gc.ca/climate\\_normals/index\\_e.html](http://climate.weather.gc.ca/climate_normals/index_e.html) (accessed 15 September 2016).
- Fang C, Moncrieff JB (2001) The dependence of soil CO<sub>2</sub> efflux on temperature. *Soil Biology and Biochemistry*, **33**, 155–165.
- Finger RA, Turetsky MR, Kielland K, Ruess RW, Mack MC, Euskirchen ES (2016) Effects of permafrost thaw on nitrogen availability and plant-soil interactions in a boreal Alaskan lowland. *Journal of Ecology*, **194**, 1542–1554.
- Friedlingstein P, Andrew RM, Rogelj J et al. (2014a) Persistent growth of CO<sub>2</sub> emissions and implications for reaching climate targets. *Nature Geoscience*, **7**, 709–715.
- Friedlingstein P, Meinshausen M, Arora VK, Jones CD, Anav A, Liddicoat SK, Knutti R (2014b) Uncertainties in CMIP5 climate projections due to carbon cycle feedbacks. *Journal of Climate*, **27**, 511–526.
- Frolking S, Roulet N, Fuglestad J (2006) How northern peatlands influence the Earth's radiative budget: Sustained methane emission versus sustained carbon sequestration. *Journal of Geophysical Research*, **111**, G01008.
- Garon-Labrecque M-E, Léveillé-Bourret É, Higgins K, Sonnentag O (2015) Additions to the Boreal Flora of the Northwest Territories with a Preliminary Vascular Flora of Scotty Creek. *Canadian Field-Naturalist*, **129**, 349–367.
- Gea-Izquierdo G, Makela A, Margolis HA et al. (2010) Modeling acclimation of photosynthesis to temperature in evergreen conifer forests. *New Phytologist*, **188**, 175–186.
- Girardin MP, Hogg EH, Bernier PY, Kurz WA, Guo XJ, Cyr G (2016) Negative impacts of high temperatures on growth of black spruce forests intensify with the anticipated climate warming. *Global Change Biology*, **22**, 627–643.
- Grant RF, Margolis HA, Barr AG, Black TA, Dunn AL, Bernier PY, Bergeron O (2009) Changes in net ecosystem productivity of boreal black spruce stands in response to changes in temperature at diurnal and seasonal time scales. *Tree Physiology*, **29**, 1–17.
- Hadden D, Grelle A (2016) Changing temperature response of respiration turns boreal forest from carbon sink into carbon source. *Agricultural and Forest Meteorology*, **223**, 30–38.
- Hanis KL, Amiro BD, Tenuta M et al. (2015) Carbon exchange over four growing seasons for a subarctic sedge fen in northern Manitoba, Canada. *Arctic Science*, **1**, 27–44.
- Heijmans MMPD, Klees H, De Visser W, Berendse F (2002) Response of a Sphagnum bog plant community to elevated CO<sub>2</sub> and N supply. *Plant Ecology*, **162**, 123–134.
- Helbig M, Chasmer LE, Kljun N, Quinton WL, Treat CC, Sonnentag O (in press) The positive net radiative forcing of increasing methane emissions from a thawing boreal forest-wetland

landscape. *Global Change Biology*, doi: 10.1111/gcb.13520.

- Helbig M, Pappas C, Sonnentag O (2016a) Permafrost thaw and wildfire: equally important drivers of boreal tree cover changes in the Taiga Plains, Canada. *Geophysical Research Letters*, **43**, 1598–1606.
- Helbig M, Wischniewski K, Kljun N, Chasmer LE, Quinton WL, Detto M, Sonnentag O (2016b) Regional atmospheric cooling and wetting effect of permafrost thaw-induced boreal forest loss. *Global Change Biology*, doi: 10.1111/gcb.13348.
- Helbig M, Wischniewski K, Gosselin GH et al. (2016c) Addressing a systematic bias in carbon dioxide flux measurements with the EC150 and the IRGASON open-path gas analyzers. *Agricultural and Forest Meteorology*, **228–229**, 349–359.
- Hogg EH, Lieffers VJ, Wein RW (1992) Potential carbon losses from peat profiles: effects of temperature, drought cycles, and fire. *Ecological Applications*, **2**, 298–306.
- Hugelius G, Bockheim JG, Camill P et al. (2013) A new data set for estimating organic carbon storage to 3 m depth in soils of the northern circumpolar permafrost region. *Earth System Science Data*, **5**, 393–402.
- Huxman TE, Turnipseed AA, Sparks JP, Harley PC, Monson RK (2003) Temperature as a control over ecosystem CO<sub>2</sub> fluxes in a high-elevation, subalpine forest. *Oecologia*, **134**, 537–546.
- Janssens IA, Lankreijer H, Matteucci G et al. (2001) Productivity overshadows temperature in determining soil and ecosystem respiration across European forests. *Global Change Biology*, **7**, 269–278.
- Johnston CE, Ewing SA, Harden JW et al. (2014) Effect of permafrost thaw on CO<sub>2</sub> and CH<sub>4</sub> exchange in a western Alaska peatland chronosequence. *Environmental Research Letters*, **9**, 85004.
- Jones MC, Booth RK, Yu Z, Ferry P (2013) A 2200-year record of permafrost dynamics and carbon cycling in a collapse-scar bog, interior Alaska. *Ecosystems*, **16**, 1–19.
- Jones MC, Harden J, O'Donnell J, Manies K, Jorgenson T, Treat C, Ewing S (2016) Rapid carbon loss and slow recovery following permafrost thaw in boreal peatlands. *Global Change Biology*, doi:10.1111/gcb.13403.
- Kettunen A (2003) Connecting methane fluxes to vegetation cover and water table fluctuations at microsite level: A modeling study. *Global Biogeochemical Cycles*, **17**, 1051.
- Keuper F, van Bodegom PM, Dorrepaal E, Weedon JT, van Hal J, van Logtestijn RSP, Aerts R (2012) A frozen feast: thawing permafrost increases plant-available nitrogen in subarctic peatlands. *Global Change Biology*, **18**, 1998–2007.
- Kirtman B, Power SB, Adedoyin JA et al. (2013) Near-term Climate Change: Projections and Predictability. In: *Climate Change 2013: The Physical Science Basis. Contribution of Working Group I to the Fifth Assessment Report of the Intergovernmental Panel on Climate Change* (eds Stocker TF, Qin D, Plattner G-K, Tignor M, Allen SK, Boschung J, Nauels A, Xia Y, Bex V, Midgley PM), pp. 953–1028. Cambridge University Press, Cambridge, United Kingdom and New York, NY, USA.
- Kljun N, Black TA, Griffis TJ et al. (2007) Response of net ecosystem productivity of three

boreal forest stands to drought. *Ecosystems* **10**, 1039–1055.

Kljun N, Calanca P, Rotach MW, Schmid HP (2015) A simple two-dimensional parameterisation for Flux Footprint Predictions (FFP). *Geoscientific Model Development*, **8**, 3695–3713.

Knoblauch C, Beer C, Sosnin A, Wagner D, Pfeiffer E-M (2013) Predicting long-term carbon mineralization and trace gas production from thawing permafrost of Northeast Siberia. *Global Change Biology*, **19**, 1160–1172.

Koven CD (2013) Boreal carbon loss due to poleward shift in low-carbon ecosystems. *Nature Geoscience*, **6**, 452–456.

Koven CD, Schuur EAG, Schädel C et al. (2015) A simplified, data-constrained approach to estimate the permafrost carbon – climate feedback. *Philosophical Transactions of the Royal Society A*, **373**, 20140423.

Kroner Y, Way DA (2016) Carbon fluxes acclimate more strongly to elevated growth temperatures than to elevated CO<sub>2</sub> concentrations in a northern conifer. *Global Change Biology*, **22**, 2913–2928.

Kurylyk BL, Hayashi M, Quinton WL, McKenzie JC, Voss CI (2016) Influence of vertical and lateral heat transfer on permafrost thaw, peatland landscape transition, and groundwater flow. *Water Resources Research*, **52**, 1286–1305.

Lafleur PM, Moore TR, Roulet NT, Frolking S (2005) Ecosystem respiration in a cool temperate bog depends on peat temperature but not water table. *Ecosystems*, **8**, 619–629.

Lara MJ, Genet H, McGuire AD et al. (2016) Thermokarst rates intensify due to climate change and forest fragmentation in an Alaskan boreal forest lowland. *Global Change Biology*, **22**, 816–829.

Lasslop G, Reichstein M, Papale D et al. (2010) Separation of net ecosystem exchange into assimilation and respiration using a light response curve approach: critical issues and global evaluation. *Global Change Biology*, **16**, 187–208.

Le Quéré C, Moriarty R, Andrew RM et al. (2015) Global Carbon Budget 2015. *Earth System Science Data*, **7**, 349–396.

Luyssaert S, Inglis I, Jung M et al. (2007) CO<sub>2</sub> balance of boreal, temperate, and tropical forests derived from a global database. *Global Change Biology*, **13**, 2509–2537.

Mahecha MD, Reichstein M, Carvalhais N et al. (2010) Global convergence in the temperature sensitivity of respiration at ecosystem level. *Science*, **329**, 838–840.

McGuire AD, Koven CD, Lawrence DM et al. (2016) Variability in the sensitivity among model simulations of permafrost and carbon dynamics in the permafrost region between 1960 and 2009. *Global Biogeochemical Cycles*, **30**, 1015–1037.

Moore TR (2003) Dissolved organic carbon in a northern boreal landscape. *Global Biogeochemical Cycles*, **17**, 1109.

Myers-Smith IH, McGuire AD, Harden JW, Chapin FS (2007) Influence of disturbance on carbon exchange in a permafrost collapse and adjacent burned forest. *Journal of Geophysical Research*, **112**, G04017.

Natali SM, Schuur EAG, Webb EE, Hicks Pries CE, Crummer KG (2014) Permafrost degradation stimulates carbon loss from experimentally warmed tundra. *Ecology*, **95**, 602–

- Novick KA, Ficklin DL, Stoy PC et al. (2016) The increasing importance of atmospheric demand for ecosystem water and carbon fluxes. *Nature Climate Change*, **6**, 1023–1027.
- Niu S, Luo Y, Fei S et al. (2011) Seasonal hysteresis of net ecosystem exchange in response to temperature change: patterns and causes. *Global Change Biology*, **17**, 3102–3114.
- Niu S, Luo Y, Fei S et al. (2012) Thermal optimality of net ecosystem exchange of carbon dioxide and underlying mechanisms. *The New Phytologist*, **194**, 775–783.
- O'Donnell JA, Jorgenson MT, Harden JW, McGuire AD, Kanevskiy MZ, Wickland KP (2012) The Effects of Permafrost Thaw on Soil Hydrologic, Thermal, and Carbon Dynamics in an Alaskan Peatland. *Ecosystems*, **15**, 213–229.
- Olefeldt D, Goswami S, Grosse G et al. (2016) Circumpolar distribution and carbon storage of thermokarst landscapes. *Nature Communications*, **7**, 13043.
- Osterkamp TE, Viereck L, Shur Y, Jorgenson MT, Racine CH, Doyle A, Boone RD (2000) Observations of Thermokarst and Its Impact on Boreal Forests in Alaska, U.S.A. *Arctic, Antarctic, and Alpine Research*, **32**, 303–315.
- Pan Y, Birdsey RA, Fang J et al. (2011) A Large and Persistent Carbon Sink in the World's Forests. *Science*, **333**, 988–994.
- Papale D, Reichstein M, Aubinet M et al. (2006) Towards a standardized processing of Net Ecosystem Exchange measured with eddy covariance technique: algorithms and uncertainty estimation. *Biogeosciences*, **3**, 571–583.
- Peichl M, Sonnentag O, Wohlfahrt G et al. (2013) Convergence of potential net ecosystem production among contrasting C3 grasslands. *Ecology Letters*, **16**, 502–512.
- Pelletier N, Talbot J, Olefeldt D, Turetsky MR, Blodau C, Sonnentag O, Quinton WL (in press) Influence of Holocene permafrost aggradation and thaw on the paleoecology and carbon storage of a peatland complex in northwestern Canada. *The Holocene*.
- Piao S, Ciais P, Friedlingstein P et al. (2008) Net carbon dioxide losses of northern ecosystems in response to autumn warming. *Nature*, **451**, 49–52.
- Quinton WL, Hayashi M, Chasmer LE (2011) Permafrost-thaw-induced land-cover change in the Canadian subarctic: implications for water resources. *Hydrological Processes*, **25**, 152–158.
- Rayment MB, Loustau D, Jarvis PJ (2002) Photosynthesis and respiration of black spruce at three organizational scales: shoot, branch and canopy. *Tree Physiology*, **22**, 219–29.
- Reichstein M, Falge E, Baldocchi D et al. (2005) On the separation of net ecosystem exchange into assimilation and ecosystem respiration: review and improved algorithm. *Global Change Biology*, **11**, 1424–1439.
- Richardson AD, Hollinger DY, Dail DB, Lee JT, Munger JW, O'Keefe J (2009) Influence of spring phenology on seasonal and annual carbon balance in two contrasting New England forests. *Tree Physiology*, **29**, 321–331.
- Richardson AD, Black TA, Ciais P et al. (2010) Influence of spring and autumn phenological transitions on forest ecosystem productivity. *Philosophical Transactions of the Royal Society B: Biological Sciences*, **365**, 3227–3246.

- Robinson D, Moore TR (1999) Carbon and peat accumulation over the past 1200 years in a landscape with discontinuous permafrost, northwestern Canada. *Global Biogeochemical Cycles*, **13**, 591–601.
- Roulet NT, Lafleur PM, Richard PJH, Moore TR, Humphreys ER, Bubier J (2007) Contemporary carbon balance and late Holocene carbon accumulation in a northern peatland. *Global Change Biology*, **13**, 397–411.
- Runkle BRK, Sachs T, Wille C, Pfeiffer E-M, Kutzbach L (2013) Bulk partitioning the growing season net ecosystem exchange of CO<sub>2</sub> in Siberian tundra reveals the seasonality of its carbon sequestration strength. *Biogeosciences*, **10**, 1337–1349.
- Scheffer M, Hirota M, Holmgren M, Van Nes EH, Chapin FS (2012) Thresholds for boreal biome transitions. *Proceedings of the National Academy of Sciences of the United States of America*, **109**, 21384–9.
- Schipperges B, Rydin H (1998) Response of photosynthesis of Sphagnum species from contrasting microhabitats to tissue water content and repeated desiccation. *New Phytologist*, **140**, 677–684.
- Schuur EAG, McGuire AD, Schädel C et al. (2015) Climate change and the permafrost carbon feedback. *Nature*, **520**, 171–179.
- Schuur EAG, Vogel JG, Crummer KG, Lee H, Sickman JO, Osterkamp TE (2009) The effect of permafrost thaw on old carbon release and net carbon exchange from tundra. *Nature*, **459**, 556–559.
- Silvola J, Alm J, Ahlholm U, Nykanen H, Martikainen PJ (1996) CO<sub>2</sub> fluxes from peat in boreal mires under varying temperature and moisture conditions. *Journal of Ecology*, **84**, 219–228.
- Tanja S, Berninger F, Vesala T et al. (2003) Air temperature triggers the recovery of evergreen boreal forest photosynthesis in spring. *Global Change Biology*, **9**, 1410–1426.
- Tarnocai C, Canadell JG, Schuur EAG, Kuhry P, Mazhitova G, Zimov S (2009) Soil organic carbon pools in the northern circumpolar permafrost region. *Global Biogeochemical Cycles*, **23**, GB2023.
- Tjoelker MG, Oleksyn J, Reich PB (1998) Seedlings of five boreal tree species differ in acclimation of net photosynthesis to elevated CO<sub>2</sub> and temperature. *Tree Physiology*, **18**, 715–726.
- Treat CC, Wollheim WM, Varner RK, Grandy AS, Talbot J, Froking S (2014) Temperature and peat type control CO<sub>2</sub> and CH<sub>4</sub> production in Alaskan permafrost peats. *Global Change Biology*, **20**, 2674–2686.
- Treat CC, Jones MC, Camill P et al. (2016) Effects of permafrost aggradation on peat properties as determined from a pan-Arctic synthesis of plant macrofossils. *Journal of Geophysical Research: Biogeosciences*, **121**, 78–94.
- Turetsky MR, Wieder RK, Williams CJ, Vitt DH (2000) Organic matter accumulation, peat chemistry, and permafrost melting in peatlands of boreal Alberta. *Écoscience*, **7**, 379–392.
- Turetsky M, Wieder K, Halsey L, Vitt DH (2002) Current disturbance and the diminishing peatland carbon sink. *Geophysical Research Letters*, **29**, 1526.
- Turetsky MR, Wieder RK, Vitt DH, Evans RJ, Scott KD (2007) The disappearance of relict



- permafrost in boreal north America: Effects on peatland carbon storage and fluxes. *Global Change Biology*, **13**, 1922–1934.
- Ueyama M, Harazono Y, Kim Y, Tanaka N (2009) Response of the carbon cycle in sub-arctic black spruce forests to climate change: Reduction of a carbon sink related to the sensitivity of heterotrophic respiration. *Agricultural and Forest Meteorology*, **149**, 582–602.
- Ueyama M, Iwata H, Harazono Y (2014) Autumn warming reduces the CO<sub>2</sub> sink of a black spruce forest in interior Alaska based on a nine-year eddy covariance measurement. *Global Change Biology*, **20**, 1161–1173.
- Ueyama M, Tahara N, Iwata H et al. (2016) Optimization of a biochemical model with eddy covariance measurements in black spruce forests of Alaska for estimating CO<sub>2</sub> fertilization effects. *Agricultural and Forest Meteorology*, **222**, 98–111.
- Way DA, Sage RF (2008) Elevated growth temperatures reduce the carbon gain of black spruce [*Picea mariana* (Mill.) B.S.P.]. *Global Change Biology*, **14**, 624–636.
- Wehr R, Munger JW, McManus JB et al. (2016) Seasonality of temperate forest photosynthesis and daytime respiration. *Nature*, **534**, 680–683.
- Welp LR, Randerson JT, Liu HP (2007) The sensitivity of carbon fluxes to spring warming and summer drought depends on plant functional type in boreal forest ecosystems. *Agricultural and Forest Meteorology*, **147**, 172–185.
- Welp LR, Patra PK, Rodenbeck C, Nemani R, Bi J, Piper SC, Keeling RF (2016) Increasing summer net CO<sub>2</sub> uptake in high northern ecosystems inferred from atmospheric inversions and comparisons to remote sensing NDVI. *Atmospheric Chemistry and Physics*, **16**, 9047–9066.
- Wickland KP, Striegl RG, Neff JC, Sachs T (2006) Effects of permafrost melting on CO<sub>2</sub> and CH<sub>4</sub> exchange of a poorly drained black spruce lowland. *Journal of Geophysical Research*, **111**, G02011.
- Wieder WR, Cleveland CC, Smith WK, Todd-Brown K (2015) Future productivity and carbon storage limited by terrestrial nutrient availability. *Nature Geoscience*, **8**, 441–U35.
- Wilby RL, Charles SP, Zorita E, Timbal B, Whetton P, Mearns LO (2004) Guidelines for Use of Climate Scenarios Developed from Statistical Downscaling Methods. Available at : <https://www.narccap.ucar.edu/doc/tgica-guidance-2004.pdf> (accessed 15 September 2016).
- Wilmking M, Juday GP, Barber VA, Zald HSJ (2004) Recent climate warming forces contrasting growth responses of white spruce at treeline in Alaska through temperature thresholds. *Global Change Biology*, **10**, 1724–1736.
- Wolf S, Keenan TF, Fisher JB et al. (2016) Warm spring reduced carbon cycle impact of the 2012 US summer drought. *Proceedings of the National Academy of Science*, **113**, 5880–5885.
- Yu Z (2006) Holocene Carbon Accumulation of Fen Peatlands in Boreal Western Canada: A Complex Ecosystem Response to Climate Variation and Disturbance. *Ecosystems*, **9**, 1278–1288.
- Yuan W, Luo Y, Liang S et al. (2011) Thermal adaptation of net ecosystem exchange. *Biogeosciences*, **8**, 1453–1463.

Yuan W, Liu S, Zhou G et al. (2007) Deriving a light use efficiency model from eddy covariance flux data for predicting daily gross primary production across biomes. *Agricultural and Forest Meteorology*, **143**, 189–207.

### Supporting information

- Fig. S1:** Friction velocity and landscape and wetland net ecosystem CO<sub>2</sub> exchange.
- Fig. S2:** Wind direction and landscape and wetland net ecosystem CO<sub>2</sub> exchange.
- Fig. S3:** Daily gross primary production (GPP), ecosystem respiration (ER), and net ecosystem CO<sub>2</sub> exchange (NEE)
- Fig. S4:** Air temperature and soil temperature, incoming shortwave radiation, and snow depth and daily liquid precipitation.
- Fig. S5:** Daily air temperature at Fort Simpson versus daily air temperature from regional climate/earth system model simulations.
- Fig. S6:** Projected end-of-the-21<sup>st</sup>-century changes in near-surface air temperature, incoming shortwave radiation, and precipitation compared to the current conditions.
- Fig. S7:** Projections of modeled monthly wetland gross primary productivity, ecosystem respiration, and net ecosystem carbon dioxide exchange at Scotty Creek.
- Fig. S8:** Current analogues of the projected end-of-the-21<sup>st</sup>-century climate at Scotty Creek for the RCP4.5 scenario and for the RCP8.5 scenario.
- Fig. S9:** Net ecosystem CO<sub>2</sub> exchange from five Earth System Model simulations from the Coupled Model Intercomparison Project (CMIP5) for the grid cell comprising Scotty Creek (61°18' N; 121°18' W).
- Fig. S10:** Mean monthly and mean annual net ecosystem CO<sub>2</sub> exchange from CarbonTracker and five ESMs for the period 2006 to 2015 for the grid cell comprising Scotty Creek.
- Tab. S1:** Best fit parameters for the models of gross primary productivity and ecosystem respiration at the landscape- and the wetland-scale.

**Tab. 1:** Mean daily net ecosystem CO<sub>2</sub> exchange (NEE<sub>LAND</sub>), gross primary productivity (GPP<sub>LAND</sub>), and ecosystem respiration (ER<sub>LAND</sub>) at landscape-level ( $\pm$  one standard deviation) for 5 °C-daily air temperature (T<sub>a</sub>) bins between 23 March 2015 and 30 August 2016. Number of days (*n*) for bins for the observation period at Scotty Creek and the percentage of days with T<sub>a</sub> within the bins at Fort Simpson between 2006 and 2015 (data from: Environment Canada, 2016; [http://climate.weather.gc.ca/climate\\_data/](http://climate.weather.gc.ca/climate_data/)).

	NEE <sub>LAND</sub> $\pm$ std $\mu\text{mol m}^{-2} \text{s}^{-1}$	GPP <sub>LAND</sub> $\pm$ std $\mu\text{mol m}^{-2} \text{s}^{-1}$	ER <sub>LAND</sub> $\pm$ std $\mu\text{mol m}^{-2} \text{s}^{-1}$	<i>n</i>	days %
T <sub>a</sub> $\leq$ -2.5 °C	+0.28 $\pm$ 0.22	0.04 $\pm$ 0.11	0.33 $\pm$ 0.17	169	45.6
-2.5 °C < T <sub>a</sub> $\leq$ 2.5 °C	+0.28 $\pm$ 0.27	0.21 $\pm$ 0.19	0.49 $\pm$ 0.22	53	8.5
2.5 °C < T <sub>a</sub> $\leq$ 7.5 °C	+0.16 $\pm$ 0.56	0.72 $\pm$ 0.68	0.88 $\pm$ 0.62	52	9.1
7.5 °C < T <sub>a</sub> $\leq$ 12.5 °C	-0.45 $\pm$ 0.65	2.26 $\pm$ 1.32	1.81 $\pm$ 1.03	63	10.5
12.5 °C < T <sub>a</sub> $\leq$ 17.5 °C	-0.67 $\pm$ 0.85	3.74 $\pm$ 1.40	3.08 $\pm$ 1.06	90	15.2
17.5 °C < T <sub>a</sub> $\leq$ 22.5 °C	-0.80 $\pm$ 0.58	4.35 $\pm$ 1.32	3.55 $\pm$ 1.07	86	9.8
T <sub>a</sub> > 22.5 °C	-0.59 $\pm$ 0.52	5.15 $\pm$ 0.59	4.56 $\pm$ 0.74	12	1.3

**Fig. 1:** (a) Oblique photograph of an actively thawing transition zone between wetland and forest. (b) Oblique photograph of the studied boreal forest-wetland landscape taken from a helicopter. Bright green areas represent visually delineated transition zones (several metres in lateral extent). (c) Land cover types in the flux footprints of the wetland (red cross) and the landscape tower (green cross): forested permafrost peat plateaus (dark green) and wetlands [collapse-scar bogs (yellow), fens (light brown), and an upland on post-glacial till (greenish yellow in the top right corner, outside the footprint)]. Wetland areas that have been converted from forested permafrost peat plateaus since 1977 (transition zones as identified using historical aerial photographs) are indicated in light green. Note that the extent of the transition zone map in (c) is limited to the east and south. Solid lines show landscape (dark green) and wetland tower (red) 90 % flux footprint climatology.

**Fig. 2:** Comparison of half-hourly net ecosystem carbon dioxide exchange at the landscape- (NEE<sub>LAND</sub>) and wetland-scale (NEE<sub>WET</sub>) for (a) all, (b) only nighttime, and (c) only daytime measurements. Data points are color-coded according to the wetland contribution to landscape flux footprints (FP<sub>WET</sub>). The solid blue and yellow lines show the total least squares regressions for low (FP<sub>WET</sub> < 50 %) and high FP<sub>WET</sub> (FP<sub>WET</sub>  $\geq$  50 %), respectively.

**Fig. 3:** (a) Daily net ecosystem carbon dioxide exchange (NEE), (b) gross primary productivity (GPP), and (c) ecosystem respiration (ER) from the wetland and landscape (including wetlands and forests) tower for individual months. Boxes show 25<sup>th</sup> and 75<sup>th</sup> percentiles; grey lines inside the boxes show medians. Monthly medians with asterisks are significantly different (Wilcoxon signed-rank test; \*  $\alpha$  = 0.05 / \*\*  $\alpha$  = 0.01 / \*\*\*  $\alpha$  = 0.001). Note that data from the wetland tower is missing for April, May, and July 2015 due to sensor malfunctioning.

**Fig. 4:** Cumulative gap-filled net ecosystem carbon dioxide exchange at the landscape- and wetland-scale ( $\Sigma$ NEE<sub>LAND</sub> &  $\Sigma$ NEE<sub>WET</sub>, solid lines). Grey shaded areas indicating 95 % confidence



intervals of  $\Sigma\text{NEE}$  between August 2015 and 2016 due to the friction velocity threshold and random errors in NEE measurements.

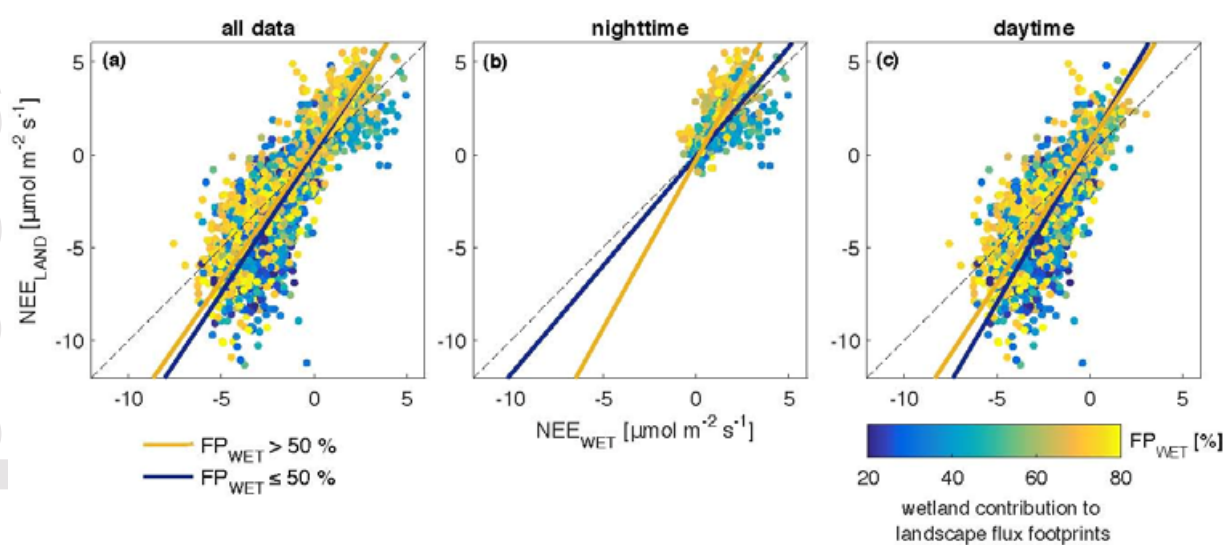
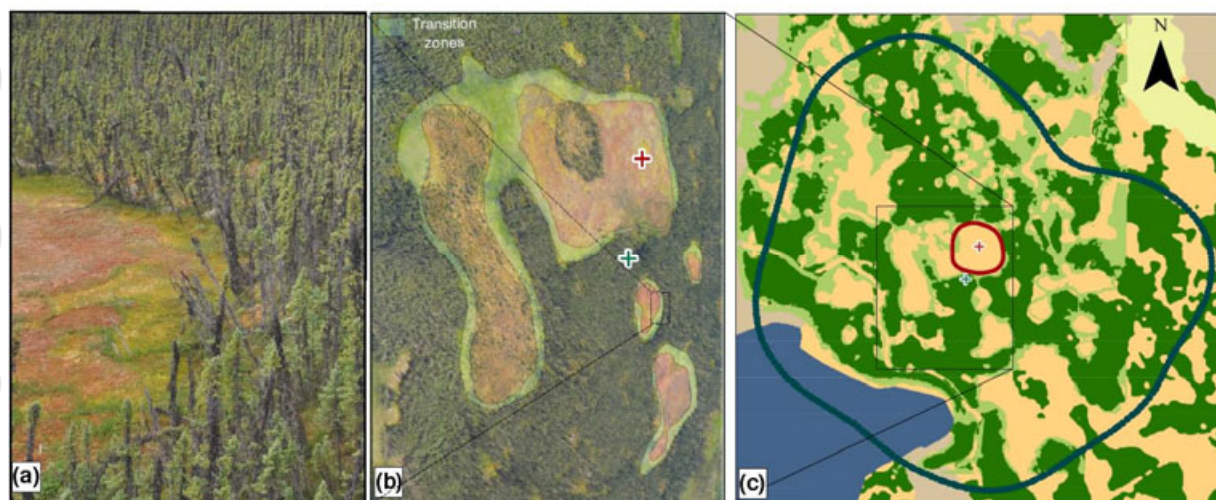
**Fig. 5:** (a) Mean daily air temperature ( $T_a$ ) and net ecosystem carbon dioxide exchange at the landscape tower ( $\text{NEE}_{\text{LAND}}$ ). Closed circles show measured  $\text{NEE}_{\text{LAND}}$  and open circles show potential NEE. Solid lines indicate the current and projected median of daily  $T_a$  between 2006-2015 and 2091-2100. Dashed lines show the respective 10<sup>th</sup> and 90<sup>th</sup> percentiles. Mean daily gross primary productivity derived from  $\text{NEE}_{\text{LAND}}$  ( $\text{GPP}_{\text{LAND}}$ ) against (b) mean daily  $T_a$  and (c) the seven-day moving average of  $T_a$ . Solid lines are best model fits to potential GPP (circles) and shaded areas indicate the 95 % confidence interval. Color-coding of data points represents mean daily incoming shortwave radiation ( $\text{SW}_{\text{in}}$ ). (d)  $\text{GPP}_{\text{LAND}}$  against  $\text{SW}_{\text{in}}$ . Color-coding shows  $T_a$ .

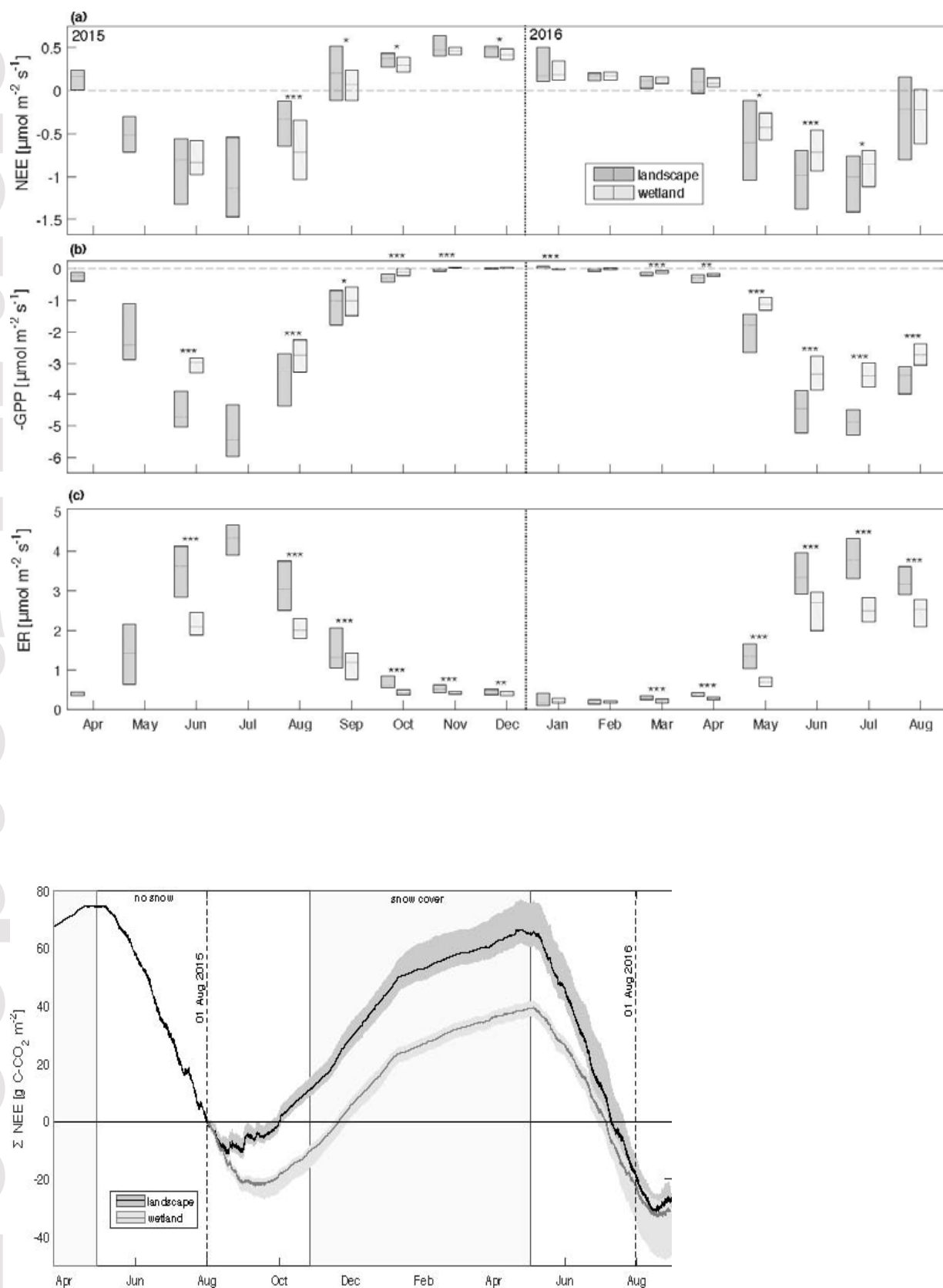
**Fig. 6:** Mean daily ecosystem respiration at the landscape tower ( $\text{ER}_{\text{LAND}}$ ) against mean daily  $T_a$ . Solid line shows the best-fit  $Q_{10}$ -model.

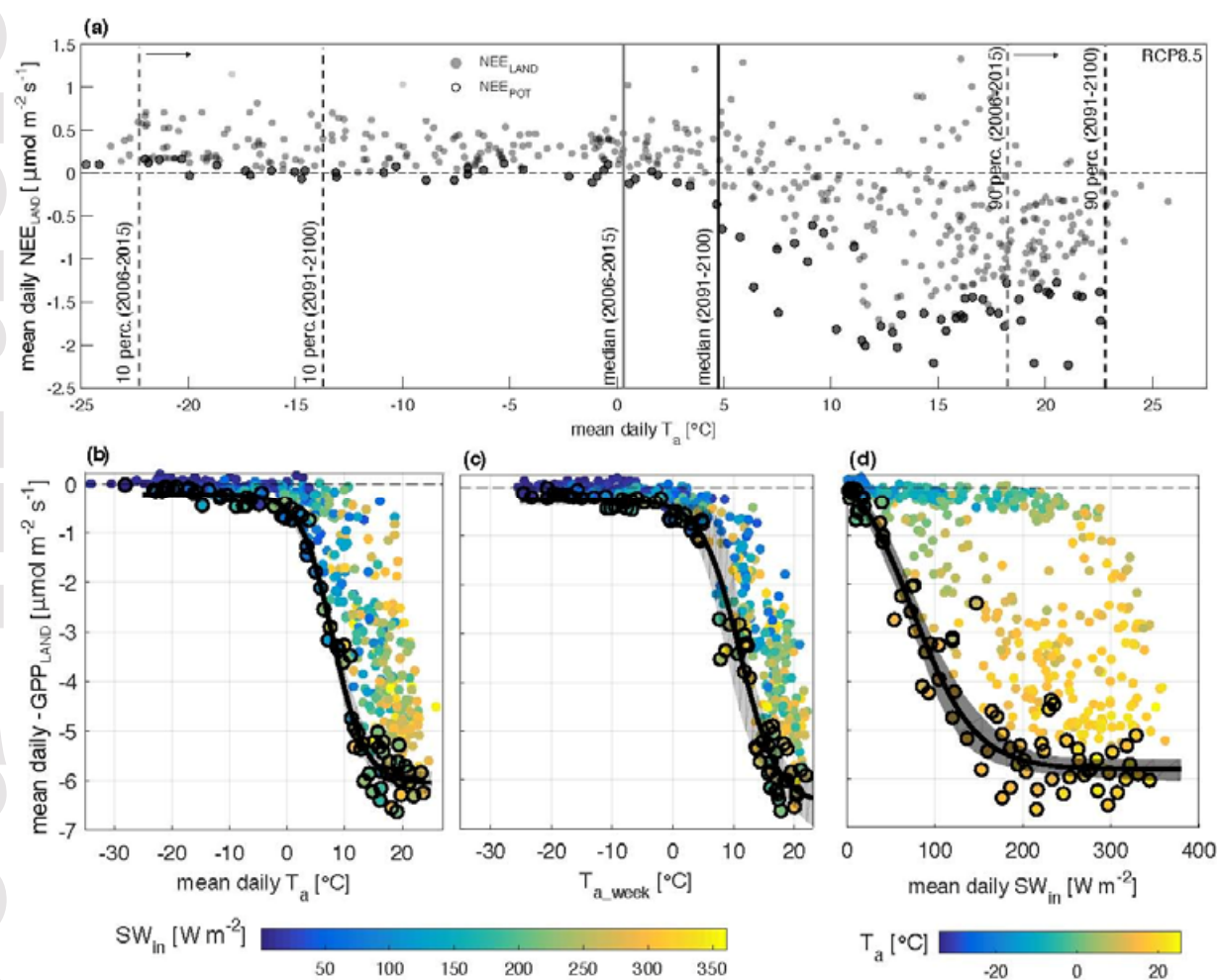
**Fig. 7:** Monthly fraction of days when potential gross primary productivity ( $\text{GPP}_{\text{POT}}$ ) is limited by (a) air temperature ( $T_a$ ), (c) incoming shortwave radiation ( $\text{SW}_{\text{in}}$ ), or (b) co-limited by both variables. The dashed line shows  $\text{GPP}_{\text{POT}}$ -limitation for  $T_a$  and  $\text{SW}_{\text{in}}$  measured at Scotty Creek between August 2015 and July 2016. Solid lines indicate ensemble mean  $\text{GPP}_{\text{POT}}$ -limitation for the recent and projected modeled  $T_a$  and  $\text{SW}_{\text{in}}$  from six combinations of four regional and three global climate models.

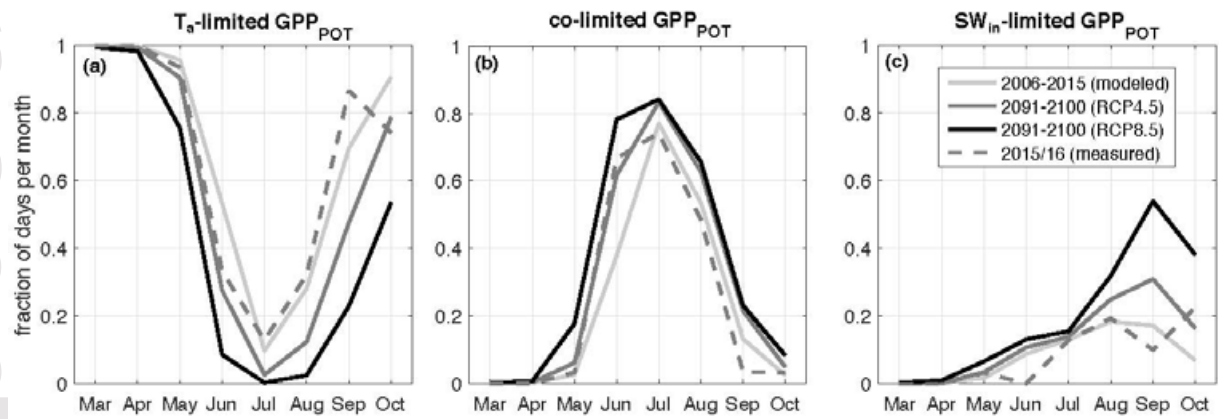
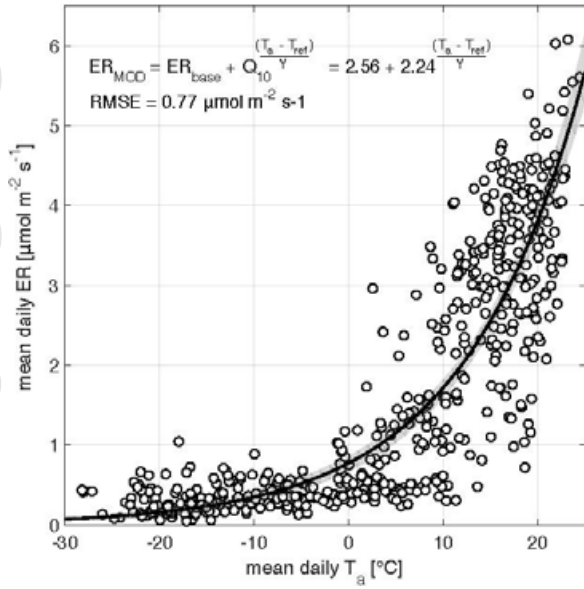
**Fig. 8:** Projections (2091-2100) of monthly modeled gross primary productivity ( $\text{GPP}_{\text{MOD}}$ ), ecosystem respiration ( $\text{ER}_{\text{MOD}}$ ), and net ecosystem carbon dioxide exchange ( $\text{NEE}_{\text{MOD}}$ ) for the landscape at Scotty Creek (a) for the RCP 4.5 and (b) for the RCP 8.5 scenario. For comparison, narrow white bars show recent (2006-2015)  $\text{GPP}_{\text{MOD}}$ ,  $\text{ER}_{\text{MOD}}$ , and  $\text{NEE}_{\text{MOD}}$ . Error bars indicate uncertainties (95 % confidence intervals) in the GPP- and ER-model.

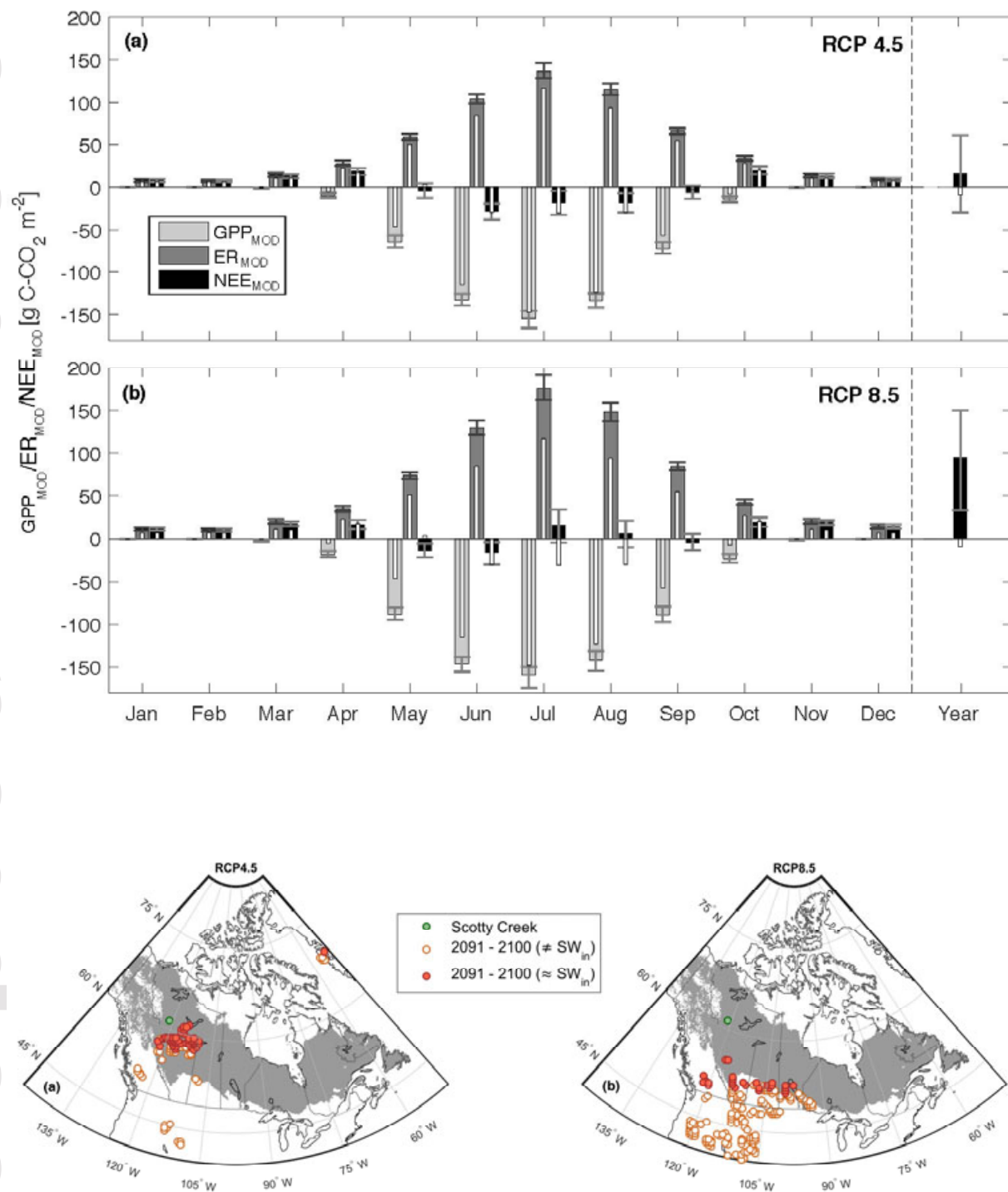
**Fig. 9:** Current climate analogues (2006-2015) of the projected end-of-21<sup>st</sup>-century (2091-2100) climate at Scotty Creek (a) for the RCP4.5 scenario and (b) for the RCP8.5 scenario. Circles show all climate analogues from six different regional/global climate model combinations. The green circle indicates the location of Scotty Creek. Orange circles show locations of current climates similar to the projected climate for Scotty Creek ( $\pm 10$  % difference in mean annual precipitation and  $\pm 0.5$  °C of mean annual air temperature). Red circles indicate locations where, additionally, differences in annual incoming shortwave radiation ( $\text{SW}_{\text{in}}$ ) are  $\pm 30$  %. Grey shaded area is the current extent of the boreal zone (data from Brandt, 2009).











This article is protected by copyright. All rights reserved.